

A DEMONSTRATION OF THE DEVON OBSERVATORY CCD
IMAGING SYSTEM'S RENDERING OF OPTICAL IMAGES
OF FAINT SNRS: CTB87

BY

STEFAN CARTLEDGE



A THESIS
SUBMITTED TO THE FACULTY OF GRADUATE STUDIES
AND RESEARCH IN PARTIAL FULFILLMENT OF THE
REQUIREMENTS FOR THE DEGREE OF MASTER OF SCIENCE
IN ASTROPHYSICS

DEPARTMENT OF PHYSICS
UNIVERSITY OF ALBERTA

EDMONTON, ALBERTA
FALL 1996



National Library
of Canada

Bibliothèque nationale
du Canada

Acquisitions and
Bibliographic Services Branch

Direction des acquisitions et
des services bibliographiques

395 Wellington Street
Ottawa, Ontario
K1A 0N4

395, rue V
Ottawa (C
K1A 0N4

Your file: Votre référence

Our file: Notre référence

The author has granted an irrevocable non-exclusive licence allowing the National Library of Canada to reproduce, loan, distribute or sell copies of his/her thesis by any means and in any form or format, making this thesis available to interested persons.

L'auteur a accordé une licence irrévocable et non exclusive permettant à la Bibliothèque nationale du Canada de reproduire, prêter, distribuer ou vendre des copies de sa thèse de quelque manière et sous quelque forme que ce soit pour mettre des exemplaires de cette thèse à la disposition des personnes intéressées.

The author retains ownership of the copyright in his/her thesis. Neither the thesis nor substantial extracts from it may be printed or otherwise reproduced without his/her permission.

L'auteur conserve la propriété du droit d'auteur qui protège sa thèse. Ni la thèse ni des extraits substantiels de celle-ci ne doivent être imprimés ou autrement reproduits sans son autorisation.

ISBN 0-612-18243-6

Canada

UNIVERSITY OF ALBERTA
LIBRARY RELEASE FORM

NAME OF AUTHOR: STEFAN CARTLEDGE

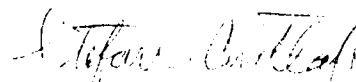
TITLE OF THESIS: A DEMONSTRATION OF THE DEVON OBSERVATORY CCD IMAGING SYSTEM'S RENDERING OF OPTICAL IMAGES OF FAINT SNRS: CTB87

DEGREE: MASTER OF SCIENCE

YEAR THIS DEGREE GRANTED: 1996

Permission is hereby granted to the University of Alberta Library to reproduce single copies of this thesis and to lend or sell such copies for private, scholarly or scientific research purposes only.

The author reserves all other publication and other rights in association with the copyright in the thesis, and except as hereinbefore provided neither the thesis nor any substantial portion thereof may be printed or otherwise reproduced in any material form whatever without the author's prior written permission.



Stefan Cartledge

6338-112 Street

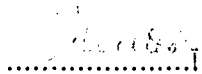
Edmonton, Alberta

T6H 3J6

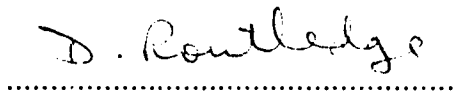
Date: *Sept. 5, 1996*

UNIVERSITY OF ALBERTA
FACULTY OF GRADUATE STUDIES AND RESEARCH

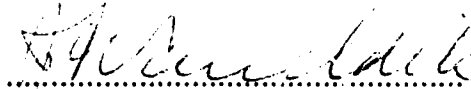
The undersigned certify that they have read, and recommend to the Faculty of Graduate Studies and Research for acceptance, a thesis entitled
A DEMONSTRATION OF THE DEVON OBSERVATORY CCD IMAGING SYSTEM'S RENDERING OF OPTICAL IMAGES OF FAINT SNRS:
CTB87 in partial fulfillment of the requirements for the degree of MASTER
OF SCIENCE IN ASTROPHYSICS.


.....

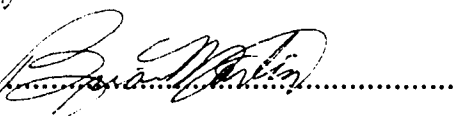
Dr. W. Jones


.....

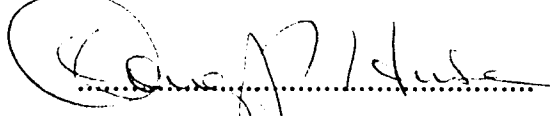
Dr. D. Routledge


.....

Dr. J. F. Vaneldik


.....

Dr. B. E. Martin


.....

Dr. D. P. Hulse

Date: September 3, 1996

ABSTRACT

The Astronomy Group at the University of Alberta is interested in using the Devon Observatory to investigate a selection of objects known at radio wavelengths that are not necessarily identified with any object visible in the optical region of the spectrum. This work describes the first test of the Observatory's ability to fulfill this task. Specifically, the first optical identification of the supernova remnant CTB87 is its subject. A detailed report is made of the procedures for acquiring and calibrating the images of CTB87. The results of surface brightness measurements are analysed and the diffuse and filamentary emission patterns of the supernova remnant are identified for future study. Sets of images are combined in mosaics which disclose information about the remnant's environment on the celestial sphere. The expected limits of the Observatory's telescope are expressed by figures for the attainable depth in magnitude for selected filters.

ACKNOWLEDGEMENTS

I would like to acknowledge the advice and support of Dr. Douglas P. Hube and Dr. Brian E. Martin, my supervisors for this project. I would also like to thank my examining committee for their help and advice, and Dr.'s Green, Gull, Seward and Wilson and Eric Steinbring for the use of their images and data. This work was funded through the University of Alberta and Dr. Hube in the form of Teaching and Research Assistantships and funds from the Natural Sciences and Engineering Research Council.

TABLE OF CONTENTS

1. INTRODUCTION AND BACKGROUND INFORMATION	
1.1 Motivation and Object Selection	1
1.2 Supernova Remnants: General	3
1.2.1 Supernovae	3
1.2.2 Supernova Remnants	6
1.2.2.a Evolution Model	6
1.2.2.b Radio Characteristics	7
1.2.2.c InfraRed Characteristics	8
1.2.2.d Optical Characteristics	8
1.2.2.e X-Ray Characteristics	9
1.2.2.f Remarks on SN and SNR Types	9
1.3 Supernova Remnants: CTB87	10
2. OBSERVATIONAL PROCEDURE AND DATA OVERVIEW	
2.1 Instrumentation and Schedule	16
2.2 General Observing Procedure	26
2.3 General Reduction Procedure	28
3. REDUCTION, ANALYSIS AND RESULTS	
3.1 Gain and Readout Noise Retrieval	30
3.2 Initial Data Reduction	30
3.3 Noise Considerations	34
3.4 Determination of Surface Brightness and the Results	37
3.5 Mosaic Construction	54
4. CONCLUSIONS	60
REFERENCES	63
APPENDICES	
Appendix A: IRAF Reduction Procedures	67
Appendix B: IRAF Photometry Procedures	71
Appendix C: IRAF Irregular Aperture Phot. Procedures	81
Appendix D: IRAF Wide-Field Synthesis	85
Appendix E: Itselect — A file manipulation Task	91

LIST OF TABLES

Table 1. Observing schedule and nightly values for chip characteristics..	18
Table 2. Signal-to-noise ratio for calibration images	36
Table 3. Signal-to-noise ratio for program field images	36
Table 4. Surface brightness values for diffuse emission and filaments	47
Table 5. Signal-to-noise ratio for diffuse emission and filaments.....	47

LIST OF FIGURES

Figure 1. Radio and X-ray images of CTB87.....	11
Figure 2. CTB87 and environs (to 2°).....	14
Figure 3. The CCD quantum efficiency as a function of wavelength.....	17
Figure 4. A zero-length exposure (before camera servicing).....	18
Figure 5. The change in CCD response linearity due to servicing.....	22
Figure 6. Full range temperature dependency of dark current.....	23
Figure 7. Temperature dependency of dark current near operating temp ...	24
Figure 8. Temperature dependency of intensity for raw calibration images..	25
Figure 9. Sample calibration images.....	32
Figure 10. Sample program fields	33
Figure 11. CTB87 through the B filter	38
Figure 12. CTB87 through the V filter	39
Figure 13. CTB87 through the H β filter.....	40
Figure 14. CTB87 through the [OIII] filter.....	41
Figure 15. A B filter image of CTB87 with stars removed.....	43
Figure 16. A V filter image of CTB87 with stars removed.....	44
Figure 17. An H β image of CTB87 with stars removed.....	45
Figure 18. An [OIII] image of CTB87 with stars removed	46
Figure 19. A B filter mosaic of the CTB87 region	55
Figure 20. A V filter mosaic of the CTB87 region	56
Figure 21. An H β filter mosaic of the CTB87 region	57
Figure 22. An [OIII] filter mosaic of the CTB87 region.....	58
Figure 23. CTB87 emission perimeters in various energy domains	62

CHAPTER ONE: INTRODUCTION AND BACKGROUND INFORMATION

1.1 MOTIVATION AND OBJECT SELECTION

The ability to study astronomical objects in distinct wavelength regions is important for understanding them more thoroughly. In accordance with this idea, many astronomical research institutions sponsor groups which work with data in different energy domains, providing a forum for discussion of studied objects from many viewpoints. At the University of Alberta, astronomers in the Department of Physics and the Department of Electrical Engineering (typically using optical and radio instruments, respectively) are cooperating in improving the observing facilities at the Devon Astronomical Observatory (latitude $53^{\circ} 23' 26.913''$ North, longitude $113^{\circ} 45' 26.914''$ West, altitude 707.9 m).

The development is being made with specific projects in mind. One proposed use of the Devon Observatory is the optical identification and observation of objects known primarily by radio wavelength observation. This use would facilitate investigations by members of the Radio Astronomy Group, removing the necessity of obtaining time at other observatories for themselves or for their collaborators. A demonstration of the applicability of the Devon Observatory to this use was required. The present work provides this demonstration in the form of the first optical detection of the supernova remnant CTB87.

The selection of this object for study was governed by several considerations. Since many interesting radio-emitting objects are extended objects¹

¹ An extended object is one in which the light observed originates from a

and the Observatory had already proven useful for studying point sources², the test object was chosen to be a galactic supernova remnant (SNR). The primary consideration for choice of SNR was its location in the sky. CTB87 (R.A. 20:14:10 Dec. +37:03, epoch 1950.0) was near Devon's zenith at the appropriate times throughout the observing run [Green, 1988].

The second determining factor was the size of the SNR. The present field-of-view of the Devon Observatory 0.5m telescope using a CCD (Charge-Coupled Device) camera (512×512 pixels) from SpectraSource Instruments and the f/8 upper end is 11.8 arcmin by 11.8 arcmin. Since many extended objects cover larger regions of the sky, the ability to create mosaics of images that could reliably mimic a larger field-of-view had to be tested. The SNR needed to be of sufficient size that it could be divided into more than one image. The SNR also needed to be sufficiently small to fit on a single image for quicker analysis³. The longest axis of CTB87 in radio images is approximately 9 arcmin. This long axis falls roughly along the diagonal in the telescope's field-of-view allowing the complete SNR to fit easily within the images.

A third consideration was the SNR's brightness. The radio objects investigated at the Devon Observatory would likely be faint objects at optical wavelengths. Also, knowledge of the detectability limits for the CCD camera would be useful in other projects. The chosen object had to be faint. CTB87

region of the celestial sphere rather than from a point.

² See Master of Science thesis *The Devon Observatory CCD Imaging System and its Application to Photometry of the Ellipsoidal Variable HR4646* by Eric Steinbring, 1995.

³ The processing and analysis time required increases at least linearly with the number of pixels involved.

was the only candidate to meet all of these requirements for the dates of the observing run.

A new upper end for the Devon Observatory telescope (f/4, prime focus) is being constructed (to be finished in summer of 1996) which will increase the field-of-view by shortening the focal length of the telescope. With the new upper end, the field-of-view will be 23.6×23.6 arcmin. This is still much smaller than many SNRs and other objects of interest. Hence, the ability to create mosaics remains a necessity.

1.2 SUPERNOVA REMNANTS: GENERAL

1.2.1 Supernovae

Supernova remnants are the products of supernova explosions, the cataclysmic “deaths” of large stars. Supernovae are generally divided into 2 classes, Type I and Type II, distinguished by their patterns of light variation and the composition of their spectra.

Type I supernovae (SNI) are very bright for roughly two weeks after the explosion, followed by an exponential decrease in light output. SNI are remarkably homogeneous in the shapes of their light curves and the absolute magnitude of their peak brightnesses. Their spectra indicate that the materials initially excited by the supernova energy are nearly consistent with a typical evolved star of at least several solar masses (M_{\odot}), with the addition of materials that might form directly and endothermically from the stellar components. The notable difference is the lack of hydrogen.

SNI occur in populations of predominantly old low-mass stars and also active star-forming regions (which include young massive stars). In addition

to their different environments, a slight distinction in the light curves⁴ of these two groups has given rise to the subclasses Type Ia and Type Ib.

Type Ia supernovae are hypothesised to result from the accretion of mass by white dwarf stars. Significant amounts of in-falling matter from a companion star can increase the internal temperature of the white dwarf enough to ignite the core. The burning of stellar materials quickly proceeds through the entirety of the star. The ignition of each layer of the star produces a shock wave. These shocks cause the white dwarf materials to erupt into an expanding supernova shell. Helium and hydrogen abundances are extremely low in the white dwarf, explaining their absence from the spectra of these supernovae.

Type Ib supernovae may be the result of evolution in a binary system containing at least one star of 8-20 M_{\odot} . Through mass-siphoning by a companion star and an ignition flash stimulated stellar wind, the surface layer of hydrogen is removed from the star as it evolves. The star continues to evolve after the loss of this layer, eventually resulting in a core collapse to a neutron star or black hole. It is expected that the remaining material expands as a supernova shell in a bounce-back reaction from the core or an off-centre explosion upon core collapse. The resulting material is deficient in hydrogen, but contains the other materials characteristic of SNI including the helium signature largely absent from SNIa. SNIb are also fainter than SNIa and are found in star-forming regions. The similarities in spectra from the two scenarios for SNI may be understood by realising that SNIb progenitors would

⁴ A light curve is the record of an object's brightness as a function of time. The distinction is in the turn-over time around maximum brightness. "Fast" SNI are generally associated with older star populations and their light curves evolve quickly. "Slow" SNI occur typically in or near star-forming regions.

evolve to white dwarfs if they did not already have the extra mass to take them beyond the white dwarf stage.

Another possible progenitor for a SNIb explosion is a Wolf-Rayet star. These massive stars lose their hydrogen envelopes through normal evolution, the end result of which would be core collapse into a neutron star or black hole.

The light curve for a Type II supernova (SNII) evolves somewhat more slowly than that of SNI. The period of maximum brightness is characterised by only a slight decrease from peak intensity over a period of several tens of days. The brightness of the supernova then falls roughly exponentially. SNII are not so similar in the shape of their light curves as are SNI. The time spent near maximum light by SNII varies. Small peaks or dips at differing locations in the exponential light curve also distinguish SNII from each other. SNII occur primarily in star-forming regions (eg. in or near arms of spiral galaxies).

SNII are end-products of the evolution of very massive stars, similar to the conjecture for SNIb. The differences in spectra and light curves originate in the composition of the supernova progenitors just prior to the explosion. Progenitors of SN II retain reasonably intact surface layers of unburned hydrogen. This layer muffles the explosion and extends the duration of peak intensity emission. SNII are significantly less bright than SNI, due to the release of neutrinos as the progenitor's core collapses. When the progenitor core collapses to form a neutron star or black hole, matter falls in from the nearby layers and becomes highly compressed as it rebounds from the core. A neutrino pulse emitted from the core heats the near-core material adding to the energy this material gains in bounce-back from the core on infall. The

result is that the non-core layers of the star explode outwards to become a supernova shell.

1.2.2 Supernova Remnants

Supernova remnants are the obvious and immediate products of supernovae. They are generally distributed into three classes, distinguished by their radio-wavelength appearance. Shell-type supernova remnants resemble rings. The rings may appear distorted due to anisotropies in the interstellar medium (ISM) density. This can give the SNR the appearance of a cross-section of a collection of bubbles, or even an incomplete shell of arcs. The line-of-sight includes more of the emission region of the SNR at its edges — since the shell is very thin in comparison to its diameter — so that a spherical emission shell would appear to be a circle of emission on the sky.

Filled-centre supernova remnants (plerions) appear to be “blobs” of emission. They may be circular or distorted, like shell SNRs, due to anisotropies in the ISM. Generally the emission is peaked in intensity at the centre of the SNR. Composite SNRs are a combination of the two: a central amorphous brightness region enveloped partially or completely by a shell of emission.

1.2.2.a *Evolution Model*

Supernova remnant evolution has been divided into a sequence of several distinct phases. Following the explosion, material expands outwards at about 10^4 km/s. The expanding material may encounter a circumstellar medium (CSM) which would be material ejected from the progenitor star during its normal evolution. Proportional to its mass and size, the CSM acts as a brake on the shell material. After clearing the CSM, the tremendously high density of the expanding shell compared to that of the surrounding ISM

likens the situation to free expansion into a vacuum. This phase may last up to a few thousand years, depending on the environment in which the supernova occurred. The expanding shell begins to form a shock wave as it sweeps up dust and gas from the ISM. The shell material becomes heated and partially ionised, while the shell begins to decelerate. This stage, called the Taylor-Sedov phase, should last a few tens of thousands of years. The following phase (“snowplough”) is dominated by deceleration of the shell through conservation of momentum as dust and clouds are encountered in the ISM. The remainder of the evolution of the SNR is a slow settling into the background as emission is dominated by cooling ionised and molecular gas and the density in the wave becomes roughly equal to the local ISM density. Anisotropies in the surrounding ISM affect the expansion of the shell in different directions. The results may be radically different from a simple circular shell.

1.2.2.b *Radio Characteristics*

Supernova remnant emission in radio wavelengths is synchrotron radiation. The standard model of the production mechanism uses the electrons ionised from gas in the shell. The magnetic field of the progenitor star is preserved in the explosion. As the shock wave forms and continues expanding, turbulence is induced in the material immediately behind the shock. This material is charged, and the magnetic field becomes twisted and anisotropic due to the turbulence in the charged medium. The charged material emits partially-polarised radio waves as it is accelerated by the magnetic fields.

Emission from the central regions of a SNR is believed to require a central neutron star or black hole. The central object emits energy as a pulsar, or as jets from an accretion disk into the surrounding material that remains

after the passage of the shock wave. The charged portion of this material emits synchrotron radiation due to acceleration by magnetic fields. The central object replenishes the material with energy, so that the emission is maintained though the alternate energy source (the shock wave) recedes from the central material.

1.2.2.c *InfraRed Characteristics*

SNR infrared (IR) emissions come from dust condensed in the cooling ejecta within the SN shell and that existing in the ISM. The warm dust cools through collisions producing the observed fluxes. Primary emission regions are at the inner edge of the expanding shell. Some emitting regions may occur on the outer edge of the shock front, depending on the composition of the ISM where it encounters the front. A central power source (neutron star or black hole) will illuminate condensed-ejecta dust in the central region of the SNR.

1.2.2.d *Optical Characteristics*

SNR optical emission originates in ionised and molecular gas regions close behind the shock wave. These regions have been heated dramatically by energy from the expanding shock. The material is ejecta moving with the wave, and emits the observed energy as it cools. Lines characteristic of hydrogen, carbon, nitrogen, oxygen, sulphur, silicon, nickel and iron in varied states of ionisation show up in optical spectra (the oxygen and sulphur lines are particularly useful in distinguishing SNR from other extended objects of similar appearance). As the shock moves farther from the explosion point, interstellar clouds may be encountered. Smaller shocks are induced in these clouds and concentrated patches of emission result.

Optical emission typically appears as a collection of filamentary arcs. The

unconnected nature of the arcs is due to anisotropies in the shell material and in the ISM. In the presence of a central power source, diffuse emission also appears. As the SNR blends into the background after tens of thousands of years of expansion, these emissions are the primary optical observables.

1.2.2.e *X-Ray Characteristics*

SNR x-ray emission tends to be thermal in nature. The material behind the shock front is heated to extreme temperatures ($> 10^6\text{K}$) and thermal x-ray emission is thus detectable. However, emission is not limited to the shell in all x-ray images. In addition to the simple shell, there are 4 other categories of x-ray morphology of SNR.

X-ray filled-centre SNRs are a subgroup of radio shell SNRs. SNRs containing pulsars are distinguished by either an obvious neutron star or a bright x-ray synchrotron nebula within the shell. A non-synchrotron bright central source indicates an accretion-powered binary. The final category includes unusual x-ray appearances: amorphous or irregular emission regions across the SNR.

1.2.2.f *Remarks on SN and SNR Types*

A suggested classification system for SNRs connects the type of explosion with the resultant SNR morphology [Mathewson *et al.*, 1983a, 1983b, 1984]. This system has not yet displaced the simpler shell-plerion-composite system. Its four classes are: Balmer-dominated, oxygen-rich, plerionic-composite and evolved.

Balmer-dominated SNRs are radio shells whose optical spectra contain strong Balmer lines of hydrogen and are weak in [OIII] and SII emissions. They are attributed to SNIa explosions; the strong hydrogen lines are due to material in the CSM or ISM. The oxygen-rich class of SNR evince spectra

with strong [OIII] lines. Material from the progenitor star, not the CSM or ISM, dominates emission. This class may result from a SN1b explosion. This connection may not be real, since there does not seem to be a neutron star or black hole product connected with these SNRs. One explanation may be drifting of the explosion product with respect to the SNR, such that the neutron star or black hole is not embedded in the material that would normally be illuminated in a plerion or composite SNR. This would likely result in the observation of a percentage of these SNRs containing central objects. Hence, if the hypothesis is valid, some other mechanism must also be contributing.

The plerionic-composite class is believed to result from SNII explosions, since the central bright region requires a neutron star or black hole for energy. The existence of a shell would depend on the density of the surrounding ISM. The evolved class is composed of SNRs whose expansion velocities are very low (eg. 50-200 km/s), and whose brightnesses are low. Models of plerion and composite SNR evolution based on central neutron stars show that these SNRs eventually become shell-like in appearance. The evolved class is comprised of the end products of aging SNRs of other classes.

1.3 SUPERNOVA REMNANTS: CTB87

CTB87 is a plerion, also commonly called a “Crab-like” SNR based on similarities to the Crab Nebula SNR. Numerous investigations involving CTB87 have been made because of this resemblance, since the Crab Nebula is a prominent object that early in its study seemed unique among SNRs. Figure 1 shows the appearance of CTB87 at radio and x-ray wavelengths; the peak in radio to the west is identified as an extragalactic point source.

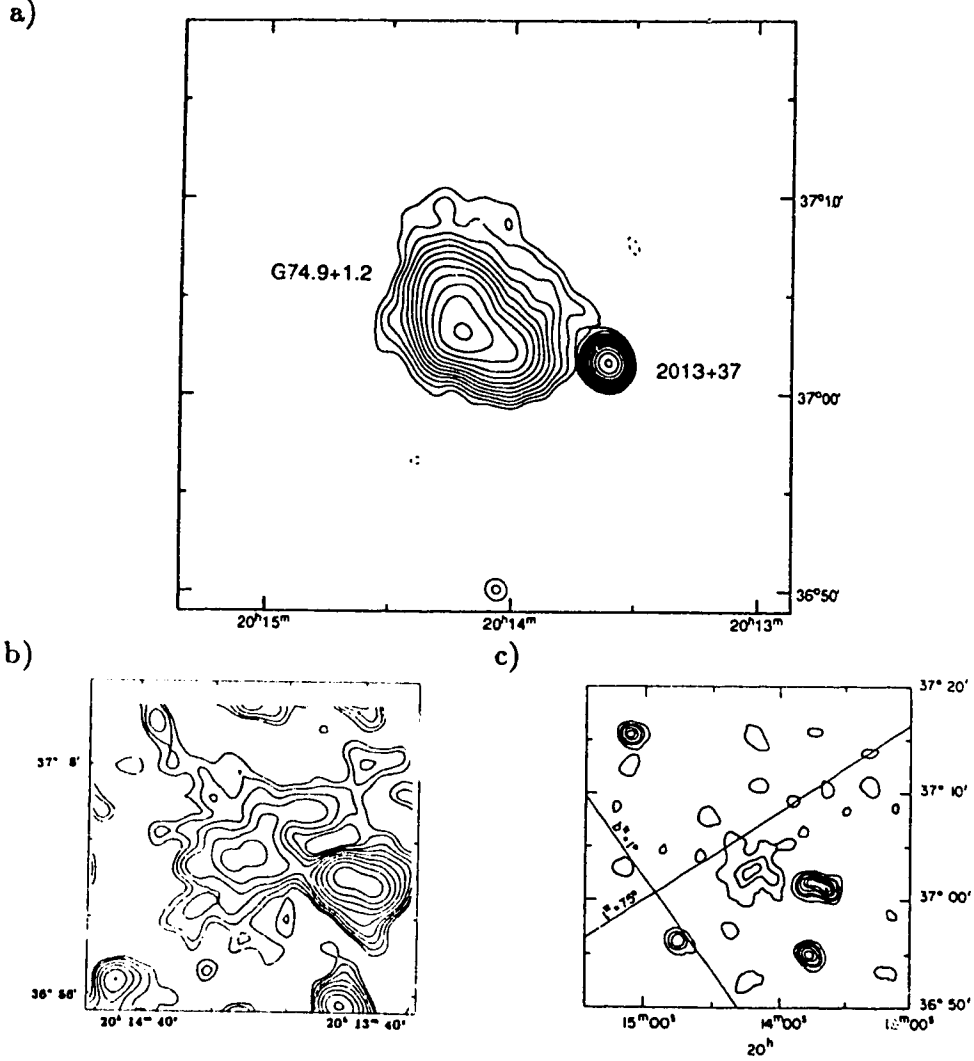


Fig. 1. Radio and x-ray images of CTB87 - a) a map of the CTB87 (G74.9+1.2) region at 1.4 GHz, HPBW is 1.4×1.2 arcmin², negative contours are dashed, positive contours are 14, 20, 28, 40 ... 640 mJy/beam [Green and Gull, 1989]; b) a 0.3-4.5 keV x-ray image with contour intensity ratio of 1.4 [Seward, 1990]; c) a processed 0.15-3.0 keV x-ray image with contour levels 5, 10, 15, 30, 45, 60, 75 counts [Wilson, 1980].

The radio structure of CTB87 is elliptical, with a slight bulge on the southeast side (the ellipse leans eastward at an angle of roughly 30° to the local hour circle). The ellipse is 9.4 arcmin by 5.9 arcmin. The spectrum of emission is a power law with a break near 11 GHz. The spectral indices above and below the frequency break are -1.02 ± 0.28 and -0.26 ± 0.10 , respectively [Kovalenko *et al.*, 1994a and 1994b]. Linear polarisation of emission at 1415

MHz is typically 5% peaking near 12% in the southwest. At 4995 MHz, typical polarisation of 15-20% peaks near 50% towards the southwest end of CTB87 [Duin *et al.*, 1975; Weiler and Shaver, 1978]. No indication of a shell of material has been observed at any frequency, presumably since an HI void roughly 500 pc across surrounds CTB87 [Green and Gull, 1989; Wallace *et al.*, 1994].

The x-ray emission from CTB87 takes the form of a synchrotron nebula 5 arcmin by 5 arcmin, whose peak lies within 30 arcsec of the peak in radio emission [Wilson, 1980]. Four point sources are nearby, one of which is identified with the extragalactic radio source 2013+370. None of the four is within the bounds of CTB87; 2013+370 is believed to be a radio galaxy at redshift (z) between 0.3 and 0.7 [Geldzahler *et al.*, 1984; Seward, 1990]. A central point source is also identified by one study [Asaoka and Koyama, 1990]. The expectation is that a central 0.1-0.2 second pulsar illuminates the nebula, but that its orientation and low luminosity preclude the observation of pulsing [Seward and Wang, 1988; Gorham *et al.*, 1996].

Studies of HI absorption of background emission indicate that CTB87 is between 11.3 and 12.5 kiloparsecs (kpc) distant [Kazès and Caswell, 1977; Green and Gull, 1989]; 12 kpc is usually taken as the actual distance. The lower limit is due to absorption noted at -65 km/s with respect to the Local Standard of Rest (LSR). A lack of strong absorption beyond -75 km/s w.r.t. LSR is taken as evidence that CTB87 is no further than the corresponding distance of 12.5 kpc (from a flat galactic rotation model). A value of 14.4 kpc was derived by applying the known radio surface brightness and angular size into curve-fitting formulae based on the empirical surface brightness-linear diameter relation [Clark and Caswell, 1976]. However, this relation is

useful only to provide “ballpark” estimates of distance⁵. A more recent paper claims, however, that CTB87 lies within a supershell around Cygnus OB1. Large ionised hydrogen velocities were measured nearby (up to -51 km/s w.r.t. LSR), that are associated with the Cygnus supershell at a distance of 1.2 - 2.3 kpc. The claim is that the HI absorption distance determination is invalid for this region [Sitnik et al., 1994]. However, this seems to be contradicted by the absence of a shell around CTB87. My conclusion is that the distance to CTB87 is still to be resolved, though its detection in this study favours a smaller distance.

At large distances, one usually needs to worry about obscuration by intervening matter. Fortunately, CTB87 lies in a direction along which extinction should not hide it from optical view [Seward, 1988]. In the direction of CTB87, IRAS data indicates dust temperature below 30K and infrared optical depth of $\sim 5.62 \times 10^{-4}$ [Odenwald and Schwartz, 1993]. Extinction is also reported to conform to the λ^{-1} dependence evident in the optical region of the spectrum. Using this relation, the optical depth near 4880Å is 0.115 and the attenuation of emission is calculated to be 0.125 magnitudes towards CTB87. Two values from the literature of total hydrogen column density towards CTB87 are $1.6 \times 10^{22} \text{cm}^{-2}$ [Seward and Wang, 1986] and $1.122 \times 10^{22} \text{cm}^{-2}$ [Asaoka and Koyama, 1990]. These correspond to visual extinctions in the range 4.5 - 12.8 magnitudes (see *The Ratio of Carbon Monoxide to Molecular Hydrogen in Interstellar Dark Clouds*, **Astrophysical Journal Supplement Series 37**, pg.407, 1978). Typical values of extinction,

⁵ The relation breaks down because of the lack of completeness of catalogues for objects of low surface brightness or small angular size. The relation may allow the determination of an upper limit on SNR distances, but this conjecture must still be proven.

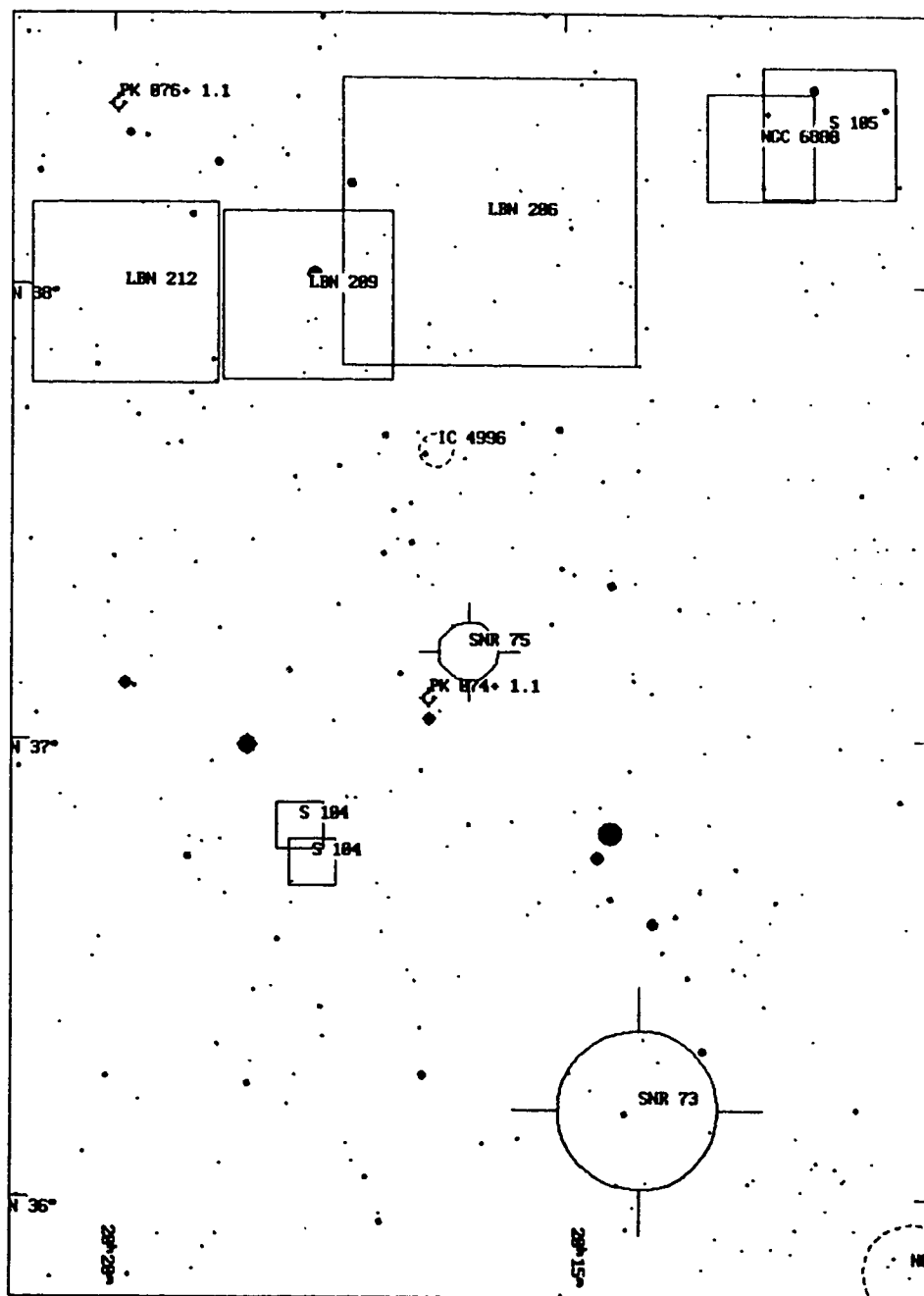


Fig. 2. CTB87 and its environs to 2° - this chart is taken the Hubble Guide Star program (Version 3.0, Project Pluto). Not shown are 4 point radio sources and 2 compact nebulosities ($< 2''$ diameter) found in a search using SIMBAD (a European astronomical database).

however, are nearer 1-1.4 mag/kpc. These values, coupled with an optical identification in this study, suggest that the HI absorption studies likely have overestimated the distance to CTB87 — unless extinction is under ~ 6 magnitudes over the 12 kpc. Nearby CO and HII clouds do not seem to hamper visibility of the SNR, nor should any nearby extended object contribute to the program images (see Figure 2). Assuming a distance of 12 kpc, CTB87 is 240 pc above the galactic plane and its physical size is 33 pc by 21 pc.

The age of CTB87 is in dispute. Its calculated size is roughly 8 times the size of the Crab Nebula in each dimension. If these SNRs are similar in nature, then CTB87 must be much older than 942 years (the Crab Nebula is the result of a supernova explosion in 1054 A.D.). The authors of a recent search for pulsars in plerions suggest that CTB87 is roughly 10,000 years old, a reasonable age considering its size relative to the Crab [Gorham *et al.*, 1996]. Assuming the total radio luminosity of the SNR is equivalent to the energy lost from a central pulsar, an age of 4000-7000 years can be derived [Wilson, 1980]. Using a formula developed from evolution theory of plerions [Weiler and Panagia, 1980], CTB87 should be about 2600 years old [Morsi and Reich, 1987]. This figure agrees with the identification of CTB87 with a supernova recorded by the Chinese in 523 B.C. [Wang *et al.*, 1986].

CHAPTER TWO: OBSERVATIONAL PROCEDURE AND DATA OVERVIEW

2.1 INSTRUMENTATION AND SCHEDULE

The Devon Astrophysical Observatory is located on University of Alberta land near the town of Devon in the Metropolitan Edmonton Area. Light pollution is not a serious problem, however astronomical seeing (resolution) is limited to 4-6 arcsec. The telescope has a 50cm aperture with interchangeable upper ends which allow the observer to choose the focal ratio. The CTB87 observations were done using the f/8 end. CCD images were taken by a SpectraSource HPC-1 Peltier-cooled CCD camera containing a Tektronix TK512 chip, mounted at the Cassegrain focus of the telescope. Figure 3 highlights the response of the chip as a function of wavelength. The f/8 end provides an 11.8 arcmin by 11.8 arcmin field of view to the 512 by 512 pixel CCD chip for a scale of $1.38 \text{ arcsec}(\text{pixel})^{-1}$. The CCD camera is operated using SpectraSource software stored on a 33 MHz 486 personal computer at the Observatory. Images are stored by the computer and transferred by tape to computers in the Avadh Bhatia Physics Building at the University of Alberta⁶, where image reduction and analysis take place.

Many problems arose after the camera was installed. Early problems of vignetting of images and telescope tracking were dealt with by careful collimation of the telescope's mirrors and adjustment of the telescope drive speed. The camera itself did not work properly. An unusual pattern was evident in zero-length exposures (see Figure 4), and the rate of absorption of

⁶ These computers are a Sun Workstation running Unix and a 100 MHz 486 personal computer usually running Linux. They are denoted STELLAR and GALAXY, respectively.

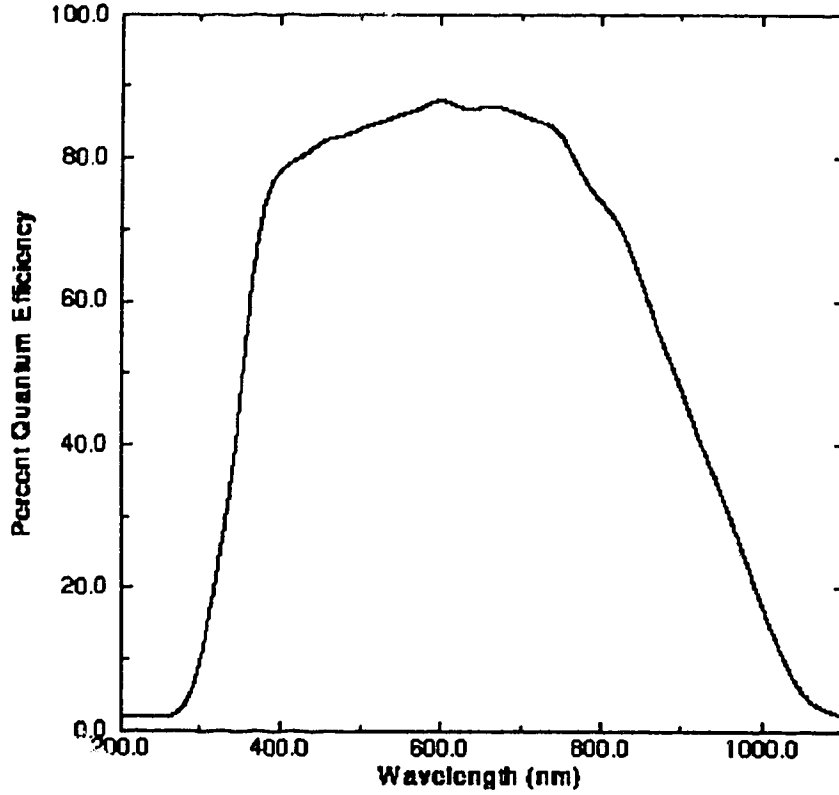


Fig. 3. A plot of the quantum efficiency of the TK512 CCD as a function of wavelength of incident light [Steinbring, 1995].

thermal energy by the chip and the chip's readout noise were extremely high. The camera was returned to SpectraSource Instruments for servicing following the completion of an ellipsoidal binary study [Steinbring, 1995]. The camera was returned to us in working condition, and observations of CTB87 began in earnest in August 1995. Table 1 details the observing schedule, noting also the CCD characteristics of gain, readnoise and available dynamic range determined for each observing session. The filter was changed between observing nights since flat fields (see §2.2) could only be taken once a night

Table 1. The observation run schedule and relevant chip characteristics.

Date	Filter	Gain (e^- /ADU)	Readnoise (e^-)	Dynamic Range (dB)
Aug 25/26, 1995	[OIII]	4.60	21.9	41.4
Sept 01/02, 1995	[OIII]	4.60	21.9	41.4
Sept 12/13, 1995	V	4.63	23.0	41.2
Sept 13/14, 1995	V	4.63	23.0	41.2
Sept 20/21, 1995	B	4.52	27.5	40.3
Sept 24/25, 1995	B	4.52	27.5	40.3
Sept 26/27, 1995	H β	4.59	27.8	40.3
Sept 29/30, 1995	H β	4.56	28.4	40.2

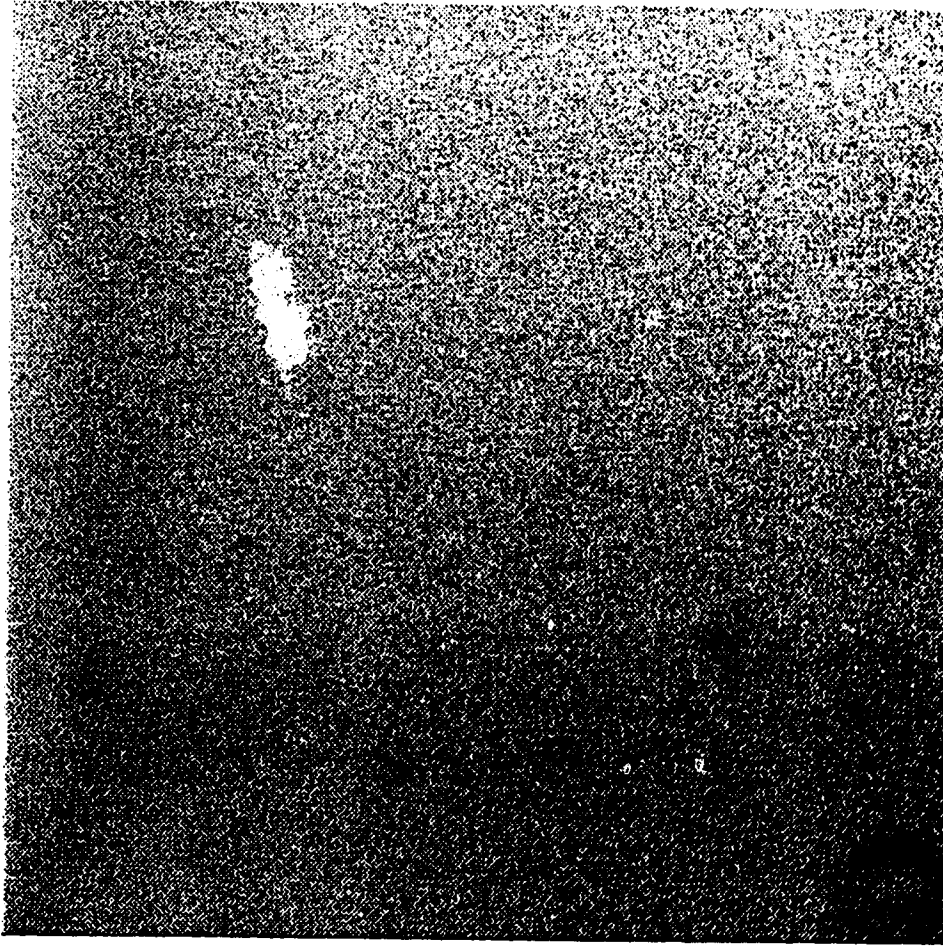


Fig. 4. A zero-length exposure taken before the CCD camera was serviced.

and the present configuration (camera and telescope) requires the removal of the camera to change the filter. The H_β and [OIII] filters were chosen since they are characteristic emission lines for supernova remnants. In particular, the [OIII] line strength is commonly used to distinguish SNR from other extended objects (eg. HII regions). These filters were standard Lumicon products (H_β centred at 486 nm with a 9 nm bandpass, [OIII] including both 496nm and 501nm lines with an 11 nm bandpass. The V and B broad-band filters (corresponding to the standard UBVRI system) should contain much of the remaining optical emission (an R filter was not available).

The CCD characteristics in Table 1 are key for accurate analysis of processed images. Gain is the number of electrons that represent an Analogue to Digital Unit, which is the unit of intensity used for storing image information. Readnoise refers to the noise introduced during the process of reading the chip and is given in electrons. The dynamic range of a CCD is a measure of the sensitivity of the chip. The Devon CCD camera stores 16-bit integer data, corresponding to a maximum of 65536 ADU/pixel. The dynamic range given is ten times the logarithm base ten of the ratio of electrons for pixel saturation ($65536 \times \text{gain}$) to the readnoise. These values were determined when the images for each session were processed at the University. The values of gain and readnoise were determined using the Image Reduction and Analysis Facility (IRAF), developed by the National Optical Astronomy Observatories (NOAO) at Tucson, Arizona in the United States. The IRAF Task⁷ used was FINDGAIN. The FINDGAIN algorithm will be discussed in §3.1. The values of gain are consistent with quotes from SpectraSource on

⁷ The IRAF program is divided into Packages, each of which contains a set of Tasks. Tasks are the operative programs that analyze or process the input images according to parameters specified at run-time.

TK512 CCD chips ($4\text{--}5\text{ e}^-/\text{ADU}$). The range $1\text{--}10\text{ e}^-/\text{ADU}$ is standard for most applications, with the sensitivity increasing as value of gain decreases. Data from recent observations of other objects indicate that the increase of readnoise evident in the table has plateaued at about 28.5 e^- . Readout noise should typically be less than 20 e^- ; SpectraSource reports that TK512 chips have readnoise of 7 e^- , specifically rating the Devon chip at 7.86 e^- at a temperature of -90°C when it was first shipped to the University of Alberta. SpectraSource also provided temperature variation curves which indicate that the measured readnoise should be 10 e^- at the present chip operating temperature. Readnoise is an intrinsic property of the chip, and should not exhibit large variations with time. The changes observed may be due to the different filters, though the reason why the filters would effect these changes is not obvious. The gain uncertainty is $0.08\text{ e}^-/\text{ADU}$ and readnoise uncertainty is 0.5 e^- . The dynamic range during the run agreed roughly with SpectraSource's tests, which quoted 40.4 dB . The specifications (readnoise) received when the camera was returned implied a readnoise of 27.5 e^- , consistent with the latest measurements. Before it was sent to SpectraSource, the chip had gain $4.9\pm0.2\text{ e}^-/\text{ADU}$, readnoise $79\pm2\text{ e}^-$ and dynamic range of $4100 = 36\text{ dB}$.

Tests of the thermal characteristics and linearity of response for the Devon CCD camera were made before the camera was sent to SpectraSource [Steinbring, 1995]. A CCD chip's response to light must be linear, ie. the gain must be constant with light intensity, to be useful. The chip must also be cooled enough that thermal energy does not significantly add to the intensity recorded by the pixels. Before the camera was returned to SpectraSource, the thermal count was 50 ADU/pixel/s . For a 500 second exposure (typical

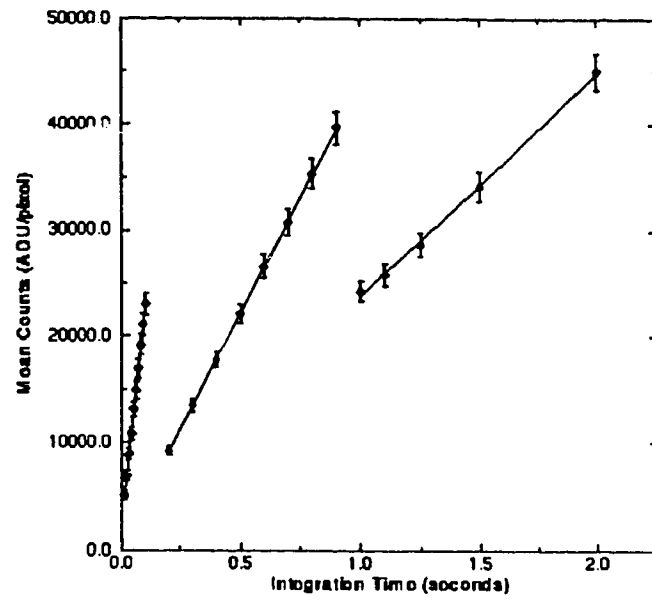
for CTB87), thermal energy took up nearly 40 percent of the chip's response capabilities. After reinstallation of the camera at Devon, the thermal count was much improved: 0.20 ADU/pixel/s for the B filter, 0.30 ADU/pixel/s for the V filter, 0.24 ADU/pixel/s for the H β filter and 0.32 ADU/pixel/s for the [OIII] filter. Figures 5 through 8 detail the thermal characteristics of the chip in comparison with those before the camera was sent to SpectraSource.

The chip temperature may be monitored using a voltmeter attached to the TEC (ThermoElectric Cooler) control unit. The potential difference reading in volts is equivalent to the Kelvin temperature of the chip in hundred's of Kelvin, with a constant offset. The ambient temperature at the time of testing was 20.0°C for a voltmeter reading of 3.048 V (304.8 K), meaning that the offset was 11.6°. All the temperatures listed in Figures 5-8 are corrected for the offset. At 20°C ambient temperature the chip operating temperature is -29.9°C. The chip temperature may be lowered past this point if the ambient temperature is lower than 20°C. During the observing run, the ambient temperature was near 0°C, and the chip was run at -32.8°C. The TEC control unit holds the temperature constant to within 0.1 K.

The linearity of the chip was tested before and after servicing by SpectraSource. This was accomplished by taking unfiltered flat field exposures⁸ at different exposure times, and ensuring that the mean intensity corresponded to an equation of the form $S - A = Bt^\alpha$, where S is the mean intensity for exposure time t , α is a constant expected to equal one and A and B are positive constants. The sequence of exposure time values in each test was the same, and the results are shown in Figure 5. Both tests confirmed the linearity of chip response for each of three regimes of exposure time: before being ser-

⁸ Flat field, dark and zero length exposures are explained in §2.2.

a.)



b.)

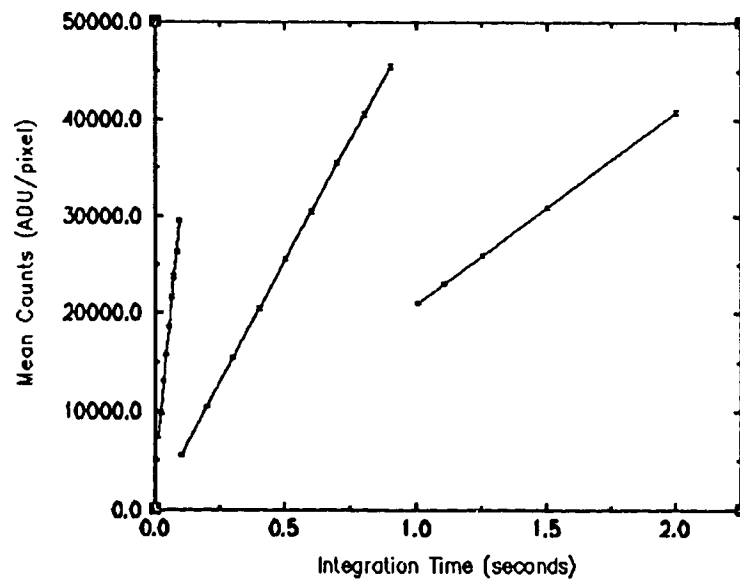
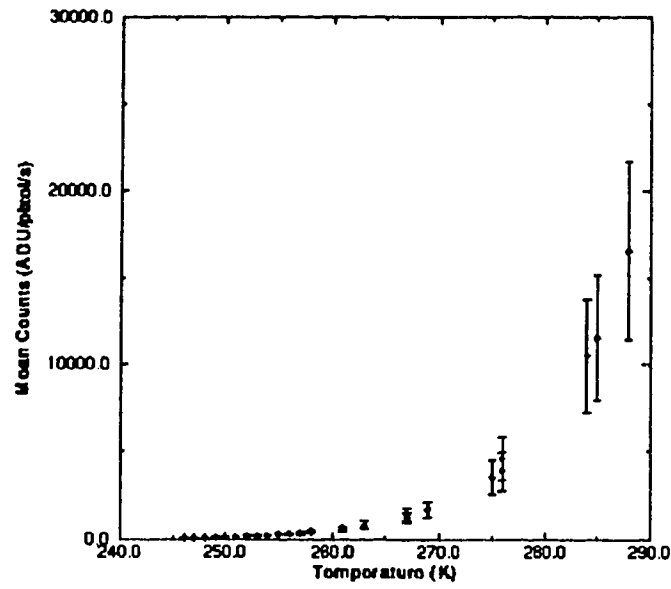


Fig. 5. The variation of mean intensity with exposure time for three different illuminations - a) before the camera was serviced [Steinbring, 1995], b) after the camera was serviced.

a)



b)

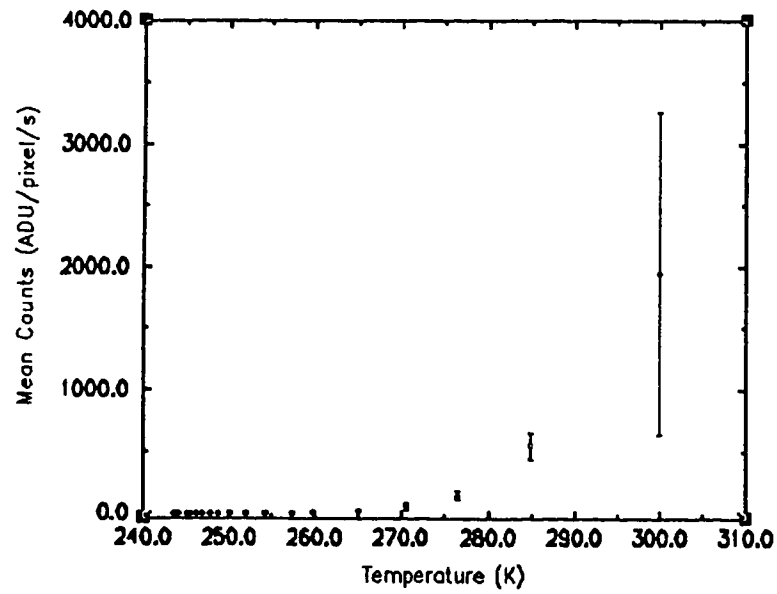
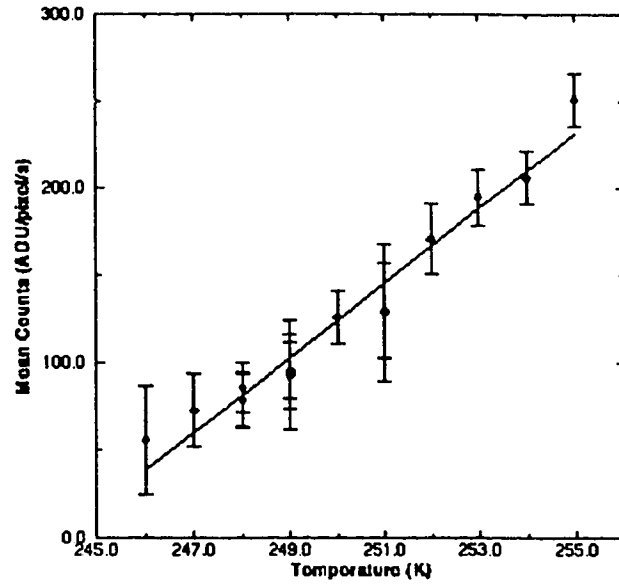


Fig. 6. The variation of mean thermal count from operating to ambient temperature - a) before the camera was serviced [Steinbring, 1995], b) after the camera was serviced.

a)



b)

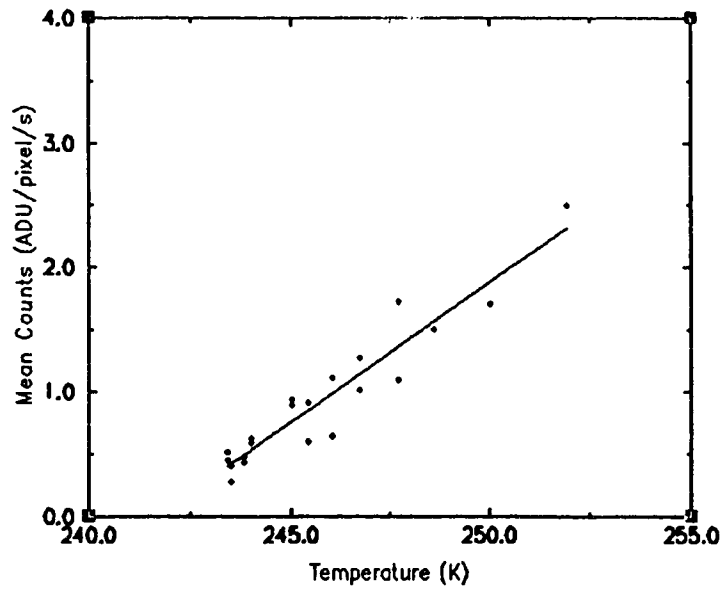
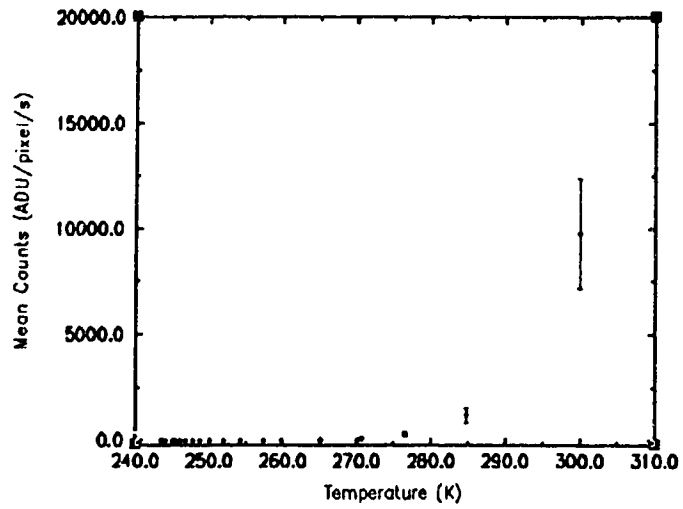


Fig. 7. The variation of mean thermal count within 12 K of operating temperature - a) before the camera was serviced, with a slope of 22 ± 1 ADU/pixel/s/K [Steinbring, 1995], b) after the camera was serviced, with a slope of 0.224 ± 0.017 ADU/pixel/s/K.

a)



b)

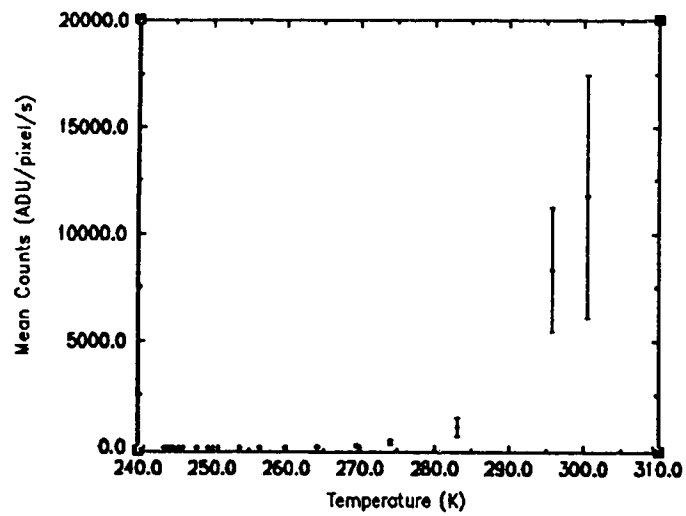


Fig. 8. The present variation of mean intensity from operating to ambient temperature - a) dark exposure variation, b) zero length exposure variation.

vice) — $\alpha = 1.036 \pm 0.009, 0.994 \pm 0.004, 0.989 \pm 0.027$; after being serviced — $\alpha = 1.013 \pm 0.014, 0.996 \pm 0.002, 1.000 \pm 0.003$. Pixel values covered the range 2,000 ADU to 65,000 ADU, including nearly the full range of the CCD.

The variation of the thermal count as the chip cooled was also investigated. The servicing of the chip by SpectraSource greatly reduced the magnitude of the thermal count, but the shape of its variation with temperature was unchanged. Figure 6 shows the complete curve from ambient temperature down to operating temperature. Figure 7 shows the region of the curve within 12 K of operating temperature, where it becomes roughly linear. Modification of the camera reduced the slope of this section from 22 ± 1 ADU/pixel/s/K to 0.224 ± 0.017 ADU/pixel/s/K. Figure 8 illustrates the variation of the unprocessed zero length and dark exposures with temperature. The zero length exposure intensities vary in a manner similar to the thermal counts, implying that the variation of dark exposure intensities is a “doubling” of this curve.

2.2 GENERAL OBSERVING PROCEDURE

In general, each observing session began at sunset. A series of twenty 2-second flat field exposures of twilight sky was stored. A flat field exposure is taken to map the apparent distribution of light on the chip when the telescope is uniformly illuminated. This map allows one to correct for pixel-to-pixel variations in the chip response and large-scale variations due to the optical path configuration of the telescope. The following steps were taken at exposure time to improve the quality of the final processed flat field at reduction time:

- The telescope drive was not activated. This ensured a new

field for every flat field exposure.

- The telescope was pointed to the east of the galactic plane. This reduced the number of stars in any field, and the Earth's rotation moved the field to sparser regions with each new exposure.
- The exposure time was set to 2 seconds to avoid serious contamination due to the "shutter effect". This is a centrally peaked light pattern, linear horizontally across the chip, caused by the finite time required to open the camera shutter [Steinbring, 1995].

The average of the 20 flat fields was used at image reduction time. Since any stars in the fields have moved between exposures and the intensity reading of their pixels is greatly different from non-star pixels, the rejection routine in the IRAF averaging Task ignores stars. The flat fields had to be acquired while the sky was bright enough to hide most of the stars, yet dim enough not to saturate the chip. The window was usually 10 to 20 minutes, and the useful range of mean intensity was between 10,000 and 40,000 ADU.

Series of ten zero-length exposures and ten 2-second dark exposures were stored. Zero-length exposures are merely readouts of the chip for an integration time of 0 seconds. The chip is not exposed to illumination, so the pixel values represent a base "bias" level, different from pixel to pixel, to which any light or thermal signal in a normal exposure would be added. The bias levels fluctuate slightly, so an average is used for reduction purposes. Dark exposures are measurements of the contribution of thermal energy to the pixel values for any normal exposure. The exposure time is flexible, since the thermal count should be linear with time. The 2-second darks were used in processing the flat fields, matching the exposure time for exactness.

After fine adjustment of the telescope's focus using a bright star, 2 dark exposures were taken. The exposure time set was the longest useful time for the filter being used for the night. The standard exposure was 180 seconds for the V filter, 300 seconds for the B filter, 400 seconds for the H_β filter and 500 seconds for the [OIII] filter. Further dark exposures were interspersed amongst the program field exposures. At these times zero-length exposures were taken as a check that nothing disastrous had occurred to the chip during the night.

The telescope was centred on CTB87 and an exposure was made. The telescope was then pointed to the northeast, northwest, southwest and southeast of the SNR, while ensuring that there was overlap between fields. The first set of images taken with each filter included a series of increasing exposure times from 15 seconds up to the maximum, all with CTB87 centred in the field. For most images, 5-10 stars in the image are overexposed and light has leaked into nearby pixels. These stellar images appear swollen, but their effect on the results is removable. The maximum exposure time was limited by these stars.

2.3 GENERAL REDUCTION PROCEDURE

Images stored on the computer were transferred to 120Mb tapes using Conner Backup Exec, and then restored to active memory on a 286 personal computer at the University of Alberta (nebula.phys.ualberta.ca). The images were then transferred by "ftp" to the Sun Workstation stellar.phys.ualberta.ca. The 486 personal computer galaxy.phys.ualberta.ca is mounted with access to STELLAR's hard drive. GALAXY is much faster than STELLAR and is equipped with a newer version of IRAF (version 2.10;

version 2.9 is used on **STELLAR**). Hence, for CTB87 data, **GALAXY** performed the processing and analysis functions, while **STELLAR** was used as a memory reservoir. **IRAF** was compiled separately for each computer due to their different internal operations. This rendered the image files used by each computer unreadable by the other. Version 2.10 also differed in that key processing Tasks were added or changed to more ably handle the data. **PSTSELECT** was a useful addition, streamlining the selection of stars to be used in **PSF**. Changes were made to **PSF** Task, allowing it to handle more variation in stellar profiles. The appendices contain more detailed information on these Tasks and their uses. These changes and the incompatibility of the two **IRAF** systems made it necessary to use only one CPU to process images.

Image data for different nights were processed separately. Images were converted to **IRAF** image format, and calibration of program fields performed using **IRAF**'s reduction package. One night's data usually consisted of 50 calibration images and 10 program images, all of which could be processed within a few hours. The time-consuming analysis procedures followed. For each program image, an accurate model of the stellar profile was created and fitted to each of the stars in the field. The stars were then removed, revealing the underlying nebulosity and filaments for brightness measurements. Program image sets with the stars intact were then overlapped to produce a mosaic.

CHAPTER THREE: REDUCTION, ANALYSIS AND RESULTS

3.1 GAIN AND READOUT NOISE RETRIEVAL

The values of gain and readout noise for the chip are important for calculating magnitude uncertainties. For each night's data, these values were determined at reduction time using the IRAF Task FINDGAIN. Table 1 (pg.16) shows that values changed significantly only when the filter was changed.

FINDGAIN uses the following algorithms:

$$gain = \frac{[\langle Flat_1 \rangle + \langle Flat_2 \rangle] - [\langle Zero_1 \rangle + \langle Zero_2 \rangle]}{[\sigma(Flat_{1-2})]^2 - [\sigma(Zero_{1-2})]^2}, \quad (1)$$

$$rdnoise = gain \times \frac{\sigma(Zero_{1-2})}{\sqrt{2}} \quad (2)$$

where $Flat_{1-2} = Flat_1 - Flat_2$, $Zero_{1-2} = Zero_1 - Zero_2$, the brackets ($\langle \rangle$) signify the mean of their argument and σ signifies standard deviation. The Task requires that the input images be unprocessed, and that the regions of the image used in the calculations have a roughly constant pixel value. A variety of pairs of flats and zeroes from amongst each night's collection of calibration images was used in the determination of the values listed in Table 1.

3.2 INITIAL DATA REDUCTION

Each night of data arrived at STELLAR in the form of 10 zero length, 10 short dark, 10 long dark, 20 flat field and roughly 10 program field exposures. All exposures were reduced using IRAF. Every image taken at Devon includes an overscan region to compensate for fluctuations in the bias level set for each exposure by the chip. The overscan is an addition to the 512×512 pixel

array. In overscan correction, the pixel values in the region are averaged, and a constant value is subtracted from each pixel in a row. The large-scale linear variation of the overscan in a column is preserved. The overscan region was then trimmed from the image. The zero length exposures were overscan corrected and averaged by ZEROCOMBINE. Averaging is done pixel by pixel: the values from each image are read and a mean and standard deviation calculated; pixel values outside 3 standard deviations from the mean are rejected; the mean is recalculated and the value saved as the signal in ADU from that pixel in the final image. This final image was used as the zero length exposure for calibrating all remaining frames.

The dark exposures were processed and averaged using DARKCOMBINE. The processing involved overscan correction and subtraction of the zero length exposure. The short darks and long darks were then averaged separately, using the same algorithm as ZEROCOMBINE. The resultant short dark image is used for the flat fields, and the resultant long dark exposure used for program exposure reductions.

The flat field images were processed using FLATCOMBINE. Flat field images are examined manually to reject any that contain very bright objects, so that the rejection routine is not compromised significantly. FLATCOMBINE then performs overscan correction, zero length exposure subtraction and short dark exposure subtraction on each image. The short dark exposure is used for consistency of exposure time. FLATCOMBINE calculated a mean intensity value for each flat field and also for these means. Each image is multiplicatively scaled so that its mean matches the average. These scaled images are operated on using the same averaging algorithm as zero length and dark exposures; the resultant image is used to correct program fields.

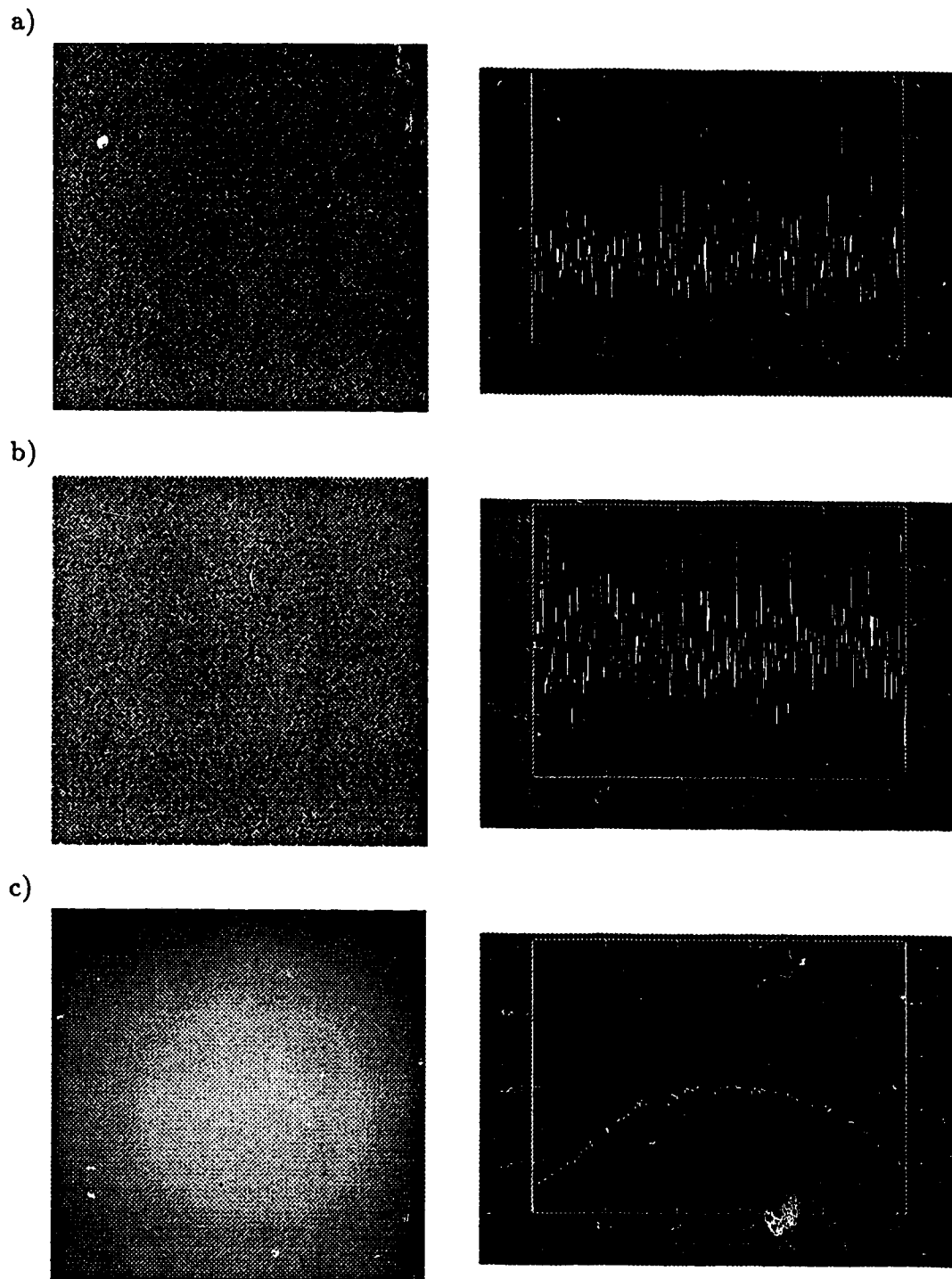
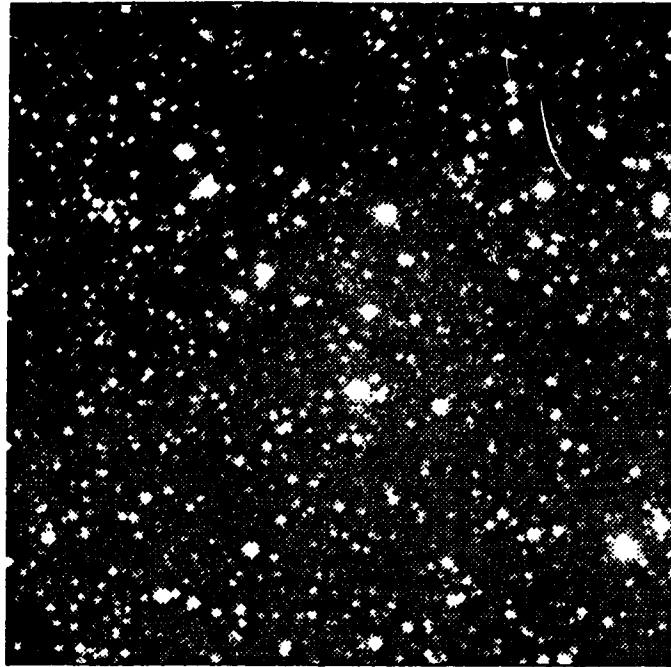


Fig. 9. Examples of each of the calibration images as viewed with SAOimage and IMPLLOT - a) a zero length exposure, b) a dark exposure, c) a flat field exposure. The IMPLLOT Task displays the intensity along one column or line of the image. These plots are of intensity along a line. The horizontal axis is the pixel number, the vertical axis is the pixel value. In a) and b), zero is the left tick mark in the midst of the values, in c) the ticks (on the left) are in 5000 ADU increments starting at 30,000 ADU.

a)



b)

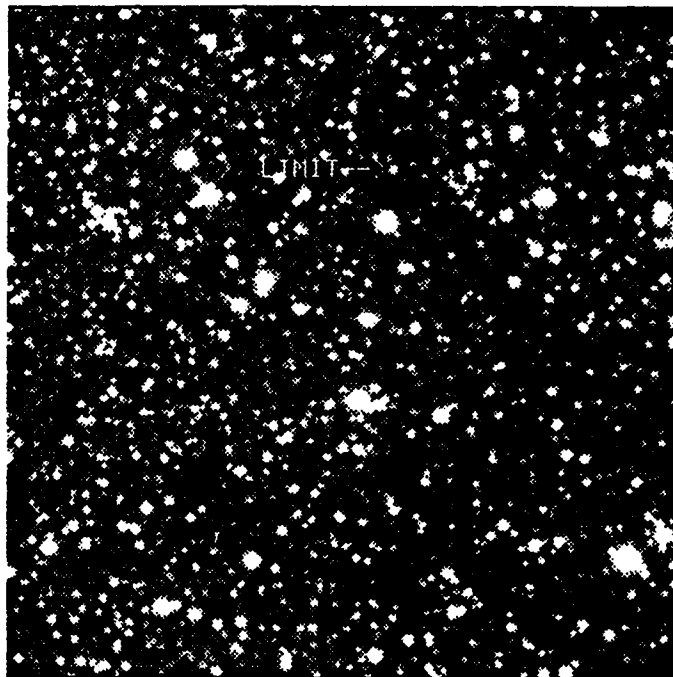


Fig. 10. Sample program field images - a) a raw image, b) a processed image. The star labeled "LIMIT" is the star used for calculating the limiting magnitude for each filter (see §3.4).

Program fields were processed using CCDPROC. Overscan correction, and zero length and long dark exposure subtraction were performed on each image. If the program field exposure was shorter than the maximum exposure time, the long dark was scaled within the Task before subtraction. CCDPROC also divided each image by the flat field, pixel by pixel, to correct for optical path focal effects. The resulting images were ready for analysis. Figure 9 provides an example of each type of calibration image and Figure 10 makes the distinction between processed and unprocessed program images obvious. For further details see Appendix A.

3.3 NOISE CONSIDERATIONS

The characteristics of the chip changed when it was serviced by Spectra-Source. The CCD chip's readout noise was reduced considerably (79 e⁻ to 23.0 e⁻ in the V filter), which increased the camera's dynamic range by ~4.5 dB. The thermal count integration rate fell from ~50 ADU/pixel/s to ~0.33 ADU/pixel/s, extending the available exposure time. These changes and a different image reduction procedure result in different processing noise figures than those previously derived for the Devon camera [Steinbring, 1995]. Some useful equations for determining the final signal to noise ratio (S/N) of an image and the objects recorded therein are:

$$\sigma_{\text{Frame}} = \frac{1}{\sqrt{2}}(\sigma_r/r)S; \quad (3)$$

$$S/N = \left[1 + \frac{\text{const}}{S_1} \right] (S/N)_1; \quad (4)$$

$$S/N = \left[S_{\text{raw}} - S_{\text{bias}} + B^2 \left(1 + \frac{1}{n_{\text{bias}}} \right) \right]^{-1/2} (S_{\text{raw}} - S_{\text{bias}}); \quad (5)$$

$$S/N = \left[\sum_{i=1}^n \left(\frac{S_i}{(S/N)_i} \right)^2 \right]^{-1/2} \sum_{i=1}^n S_i; \quad (6)$$

$$S/N = \left(1 \pm \frac{S_2}{S_1}\right) \left[1 \pm \left(\frac{S_2}{S_1}\right)^2 \left(\frac{(S/N)_1}{(S/N)_2}\right)^2\right]^{-1/2} (S/N)_1; \quad (7)$$

$$S/N = \left[1 + \left(\frac{(S/N)_1}{(S/N)_R}\right)^2\right]^{-1/2} (S/N)_1. \quad (8)$$

The equations above refer to these situations⁹:

- eq. (3) - noise for a raw image [McCall, English and Shelton, 1988]
- eq. (4) - adding a constant (+/-) to an image
- eq. (5) - subtracting a zero length exposure from a raw image
- eq. (6) - adding n like images
- eq. (7) - adding/subtracting image₂ to/from image₁
- eq. (8) - flat field correction (division)

The symbols used in these equations are defined as follows:

σ_{Frame}	the noise in a raw image (e^-/pixel)
σ_r/r	the ratio of noise to signal for a ratio of two images
S	the signal of an image (e^-/pixel)
n_{bias}	the number of zero length exposures combined in a master zero
B	the base-level noise in an image ($B = rdn_{\text{noise}}^2 + \frac{(gain^2-1)}{12} + N_o^2$)
N_o	the uncertainty in overscan constant determination

In equation (3), σ_r is the standard deviation of the pixel intensities in the ratio image, and r is their mean. Table 2 details the S/N characteristics of typical calibration images for each filter, in progressive stages of reduction. The initial S/N was estimated using equation (3) for a 50×50 pixel region near the centre of the image. The pixel intensities throughout this region were roughly uniform in all images; the pixel group was located near the apex of the flat field profile. Thus, values for S/N for the flat field images are near maximal. Individual values did not drop below 200, however, so that the

⁹ Except for (3), these equations are taken from Newberry, 1991.

Table 2. Signal to Noise Ratio as a Function of Reduction Procedures.

Filter	Image	Original	Zero Removed	Dark Removed	Combined
B	Dark	108.8	10.53	—	33.31
	Flat	460.7	477.9	477.9	2140
V	Dark	107.1	6.927	—	21.90
	Flat	310.4	320.0	320.0	1430
H_{β}	Dark	105.5	13.16	—	42.13
	Flat	459.8	493.0	493.0	2205
OIII	Dark	84.55	17.68	—	55.92
	Flat	400.0	417.5	417.5	1865

Table 3. Program Field Signal to Noise Ratio as a Function of Reduction Procedures.

Filter	Zero Removed	Dark Removed	Flat Corrected	Photon Noise
B	76.32	71.26	71.22	81.06
V	177.6	174.7	173.4	179.6
H_{β}	157.4	154.2	153.9	160.1
[OIII]	161.1	156.0	155.5	161.9

final S/N figures for each filter are reasonable estimates. The values in the remaining columns were determined by application of equations (5), (7) and (6), respectively. The value of B^2 used in equation (5) required application of equation (4) to a typical zero length exposure. The variation evident in the table is primarily due to the different light levels in each filter's bandpass.

Table 3 describes a similar progression for typical program images centred on CTB87. The S/N value due only to photon noise is listed as a comparison. All figures are derived using the mean sky value in the same pixel region used for Table 2. Image processing added 17, 31, 19 and 21 e^- to the noise in the B, V, H_{β} and [OIII] images respectively. It was noted that the combination

of photon noise and processing noise was the largest source of pixel-to-pixel variation in the sky background level: sky background standard deviation was only slightly larger than the total noise.

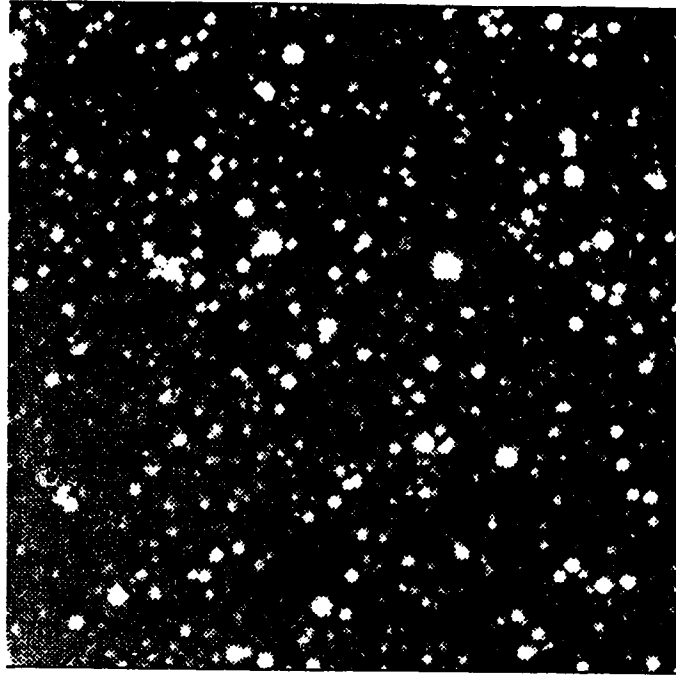
3.4 DETERMINATION OF SURFACE BRIGHTNESS AND THE RESULTS

The central image from each mosaic set mapped the full extent of CTB87, based on radio observation contours. These images are the basis for the surface brightness values listed in Table 4. Each image was initially interpreted by DAOFIND to locate all the objects in the field; input parameters for stars and sky brightness were determined using IMEXAMINE and IMSTATISTICS.

PHOT was then run on the image to obtain an estimate of the brightnesses of the identified objects. A model of a typical stellar profile (point spread function) for the image was constructed using PSF. Repeated iterations of PHOT, PSF, NSTAR and SUBSTAR were run to perfect the fit of the profile to actual stars in the image. NSTAR fit groups of selected stars and SUBSTAR removed them. Any nearby hidden objects were added to the list using PHOT. When the fits were satisfactory, ALLSTAR removed all identified objects from the image. Successive iterations of ALLSTAR removed any hidden objects. The quickest completion of this procedure took one day for one image. Often a satisfactory fit took several days. Figures 11 through 14 are typical results for each filter. Further details on the processing steps taken may be found in Appendix B.

Objects that were tentatively identified as filaments and oversaturated stars were left in the image. POLYPHOT was used to obtain instrumental magnitudes for the objects that remained. Figures 15 through 18 identify the regions that were used to construct Table 4.

a)



b)

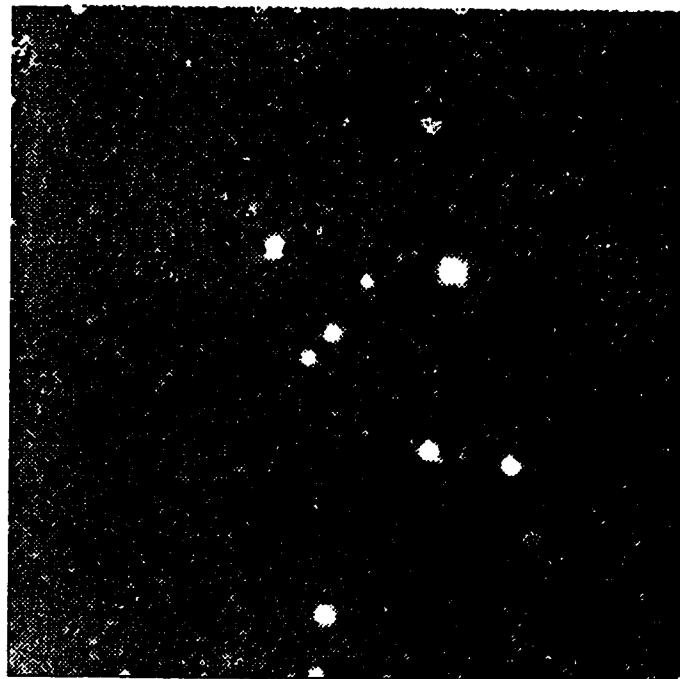
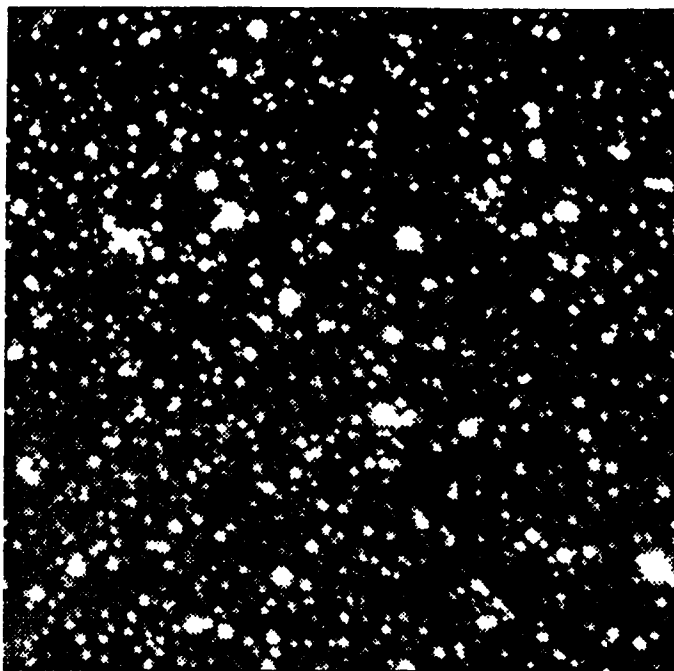


Fig. 11. A B filter image of CTB87 - a) the original, b) with stars removed.

a)



b)

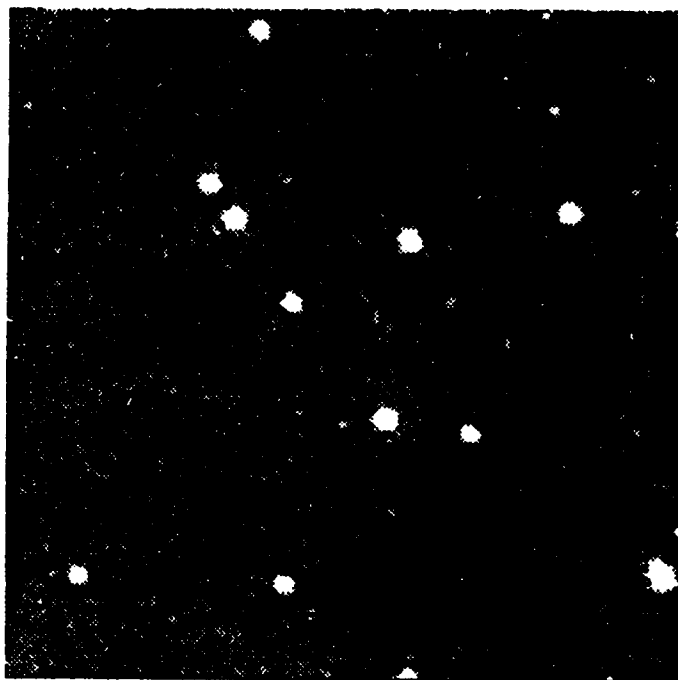
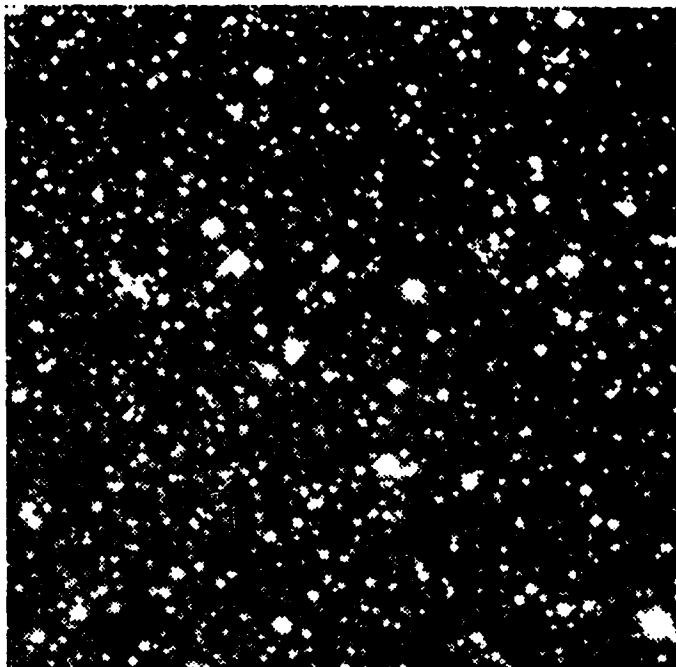


Fig. 12. A V filter image of CTB87 - a) the original, b) with stars removed.

a)



b)

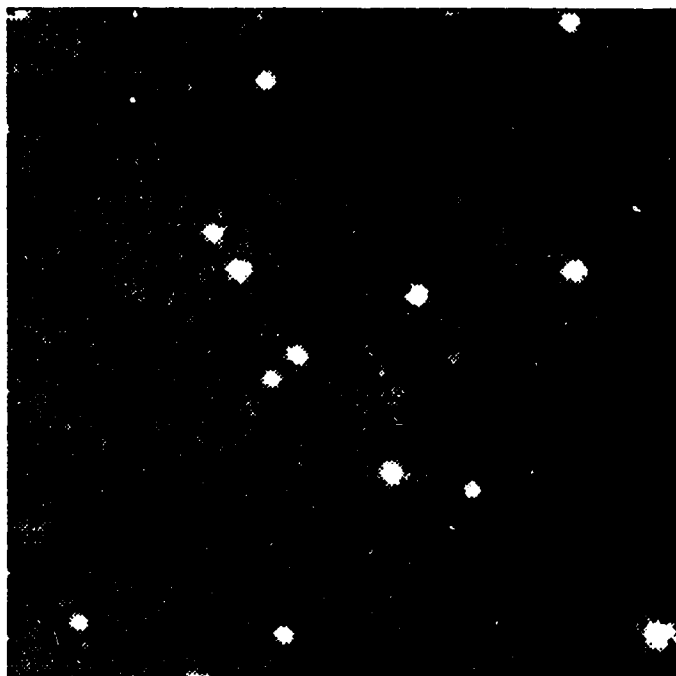
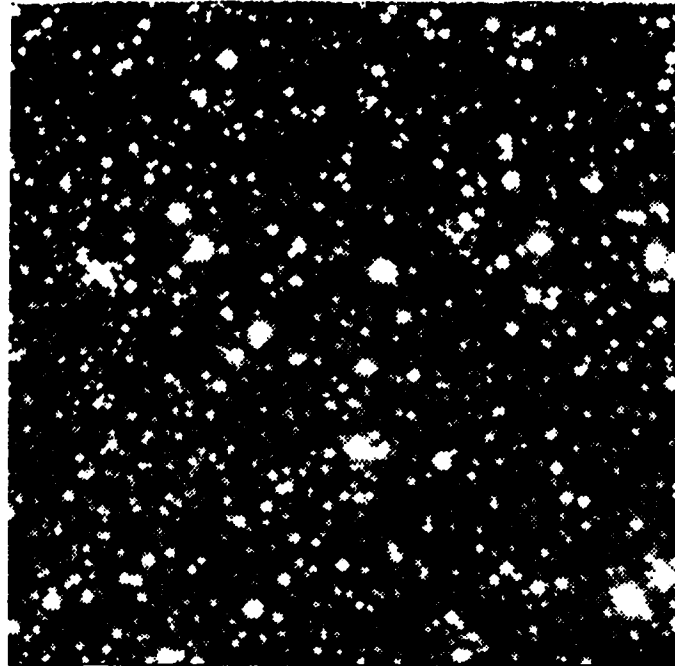


Fig. 13. An H_{α} filter image of CTB87 - a) the original, b) with stars removed.

a)



b)

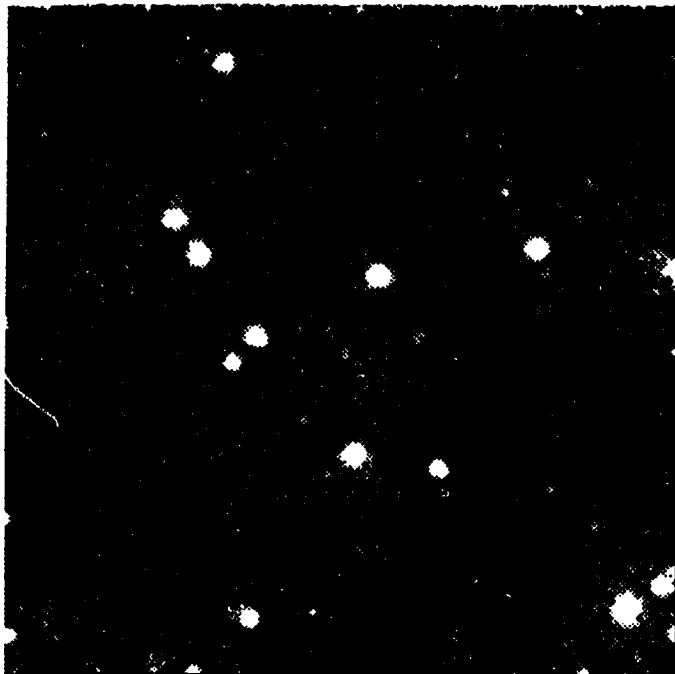


Fig. 14. An [OIII] filter image of CTB87 - a) the original, b) with stars removed.

POLYPHOT determines magnitudes by comparison of the count rate for an object with a reference level count rate (see Appendix C for details on its use). This reference level had to be calibrated to reflect actual magnitudes so that meaningful values for surface brightness could be reported. For the B, H_β and [OIII] filters, the magnitude scale was calibrated using images of M57, the Ring Nebula. M57 images were taken on the same night as each of the CTB87 observing sessions, such that M57 was at roughly the same airmass. The instrumental magnitude for M57 was compared with published values, and the reference level for POLYPHOT reset. The POLYPHOT aperture was set to mimic the size and shape of M57 from the appropriate literature source — to make the calibration as accurate as possible. A few field stars have known V magnitudes, and these were used to calibrate the V filter magnitude scale.

The reference for H_β and [OIII] magnitudes listed the flux through each filter in $\text{erg cm}^{-2} \text{sec}^{-1}$ [Lane and Pogge, 1994]. To convert these fluxes into magnitudes, the following formula was used:

$$m_{M57} = m_\odot - 2.5 \log \left(\frac{flux_{M57}}{flux_\odot} \right) \quad (9)$$

where m is apparent magnitude ($m_\odot = -26.85$ is the solar bolometric magnitude from pg. 563 of *Astrophysical Formulae* by Kenneth Lang) and $flux$ is the measured energy flux at the Earth's surface ($flux_\odot = 1.3533 \times 10^6 \text{ erg cm}^{-2} \text{sec}^{-1}$ from pg. 562 of *Astrophysical Formulae*). The magnitudes thus determined use the same flux-magnitude scale as is used for V and bolometric fluxes, a method seemingly reasonable after perusal of "Stellar Absolute Fluxes and Energy Distributions"¹⁰. The literature seems to lack reference to independent scales for H_β and [OIII] filters, which would only be different

¹⁰ By D.S. Hayes in *Calibration of Fundamental Stellar Quantities*.

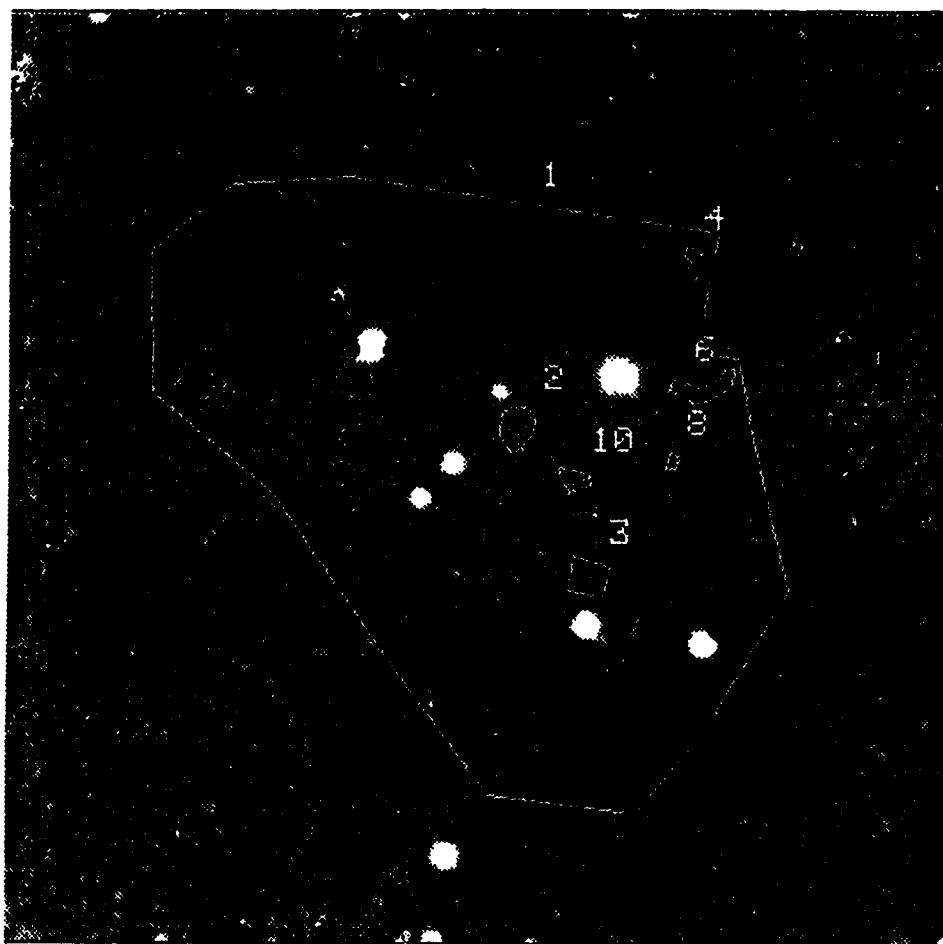


Fig. 15. A B filter image of CTB87 with the majority of stars removed. The outlined regions are those for which data are presented in Tables 4 and 5.

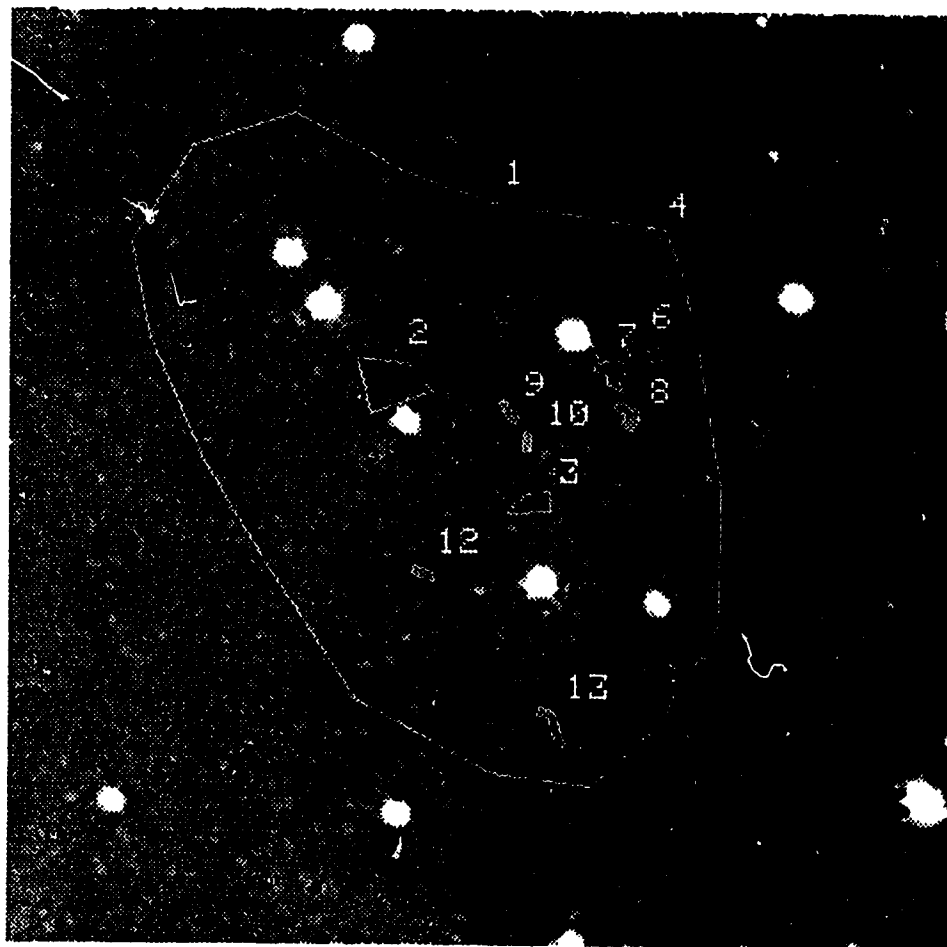


Fig. 16. A V filter image of CTB87 with the majority of stars removed. The outlined regions are those for which data are presented in Tables 4 and 5.

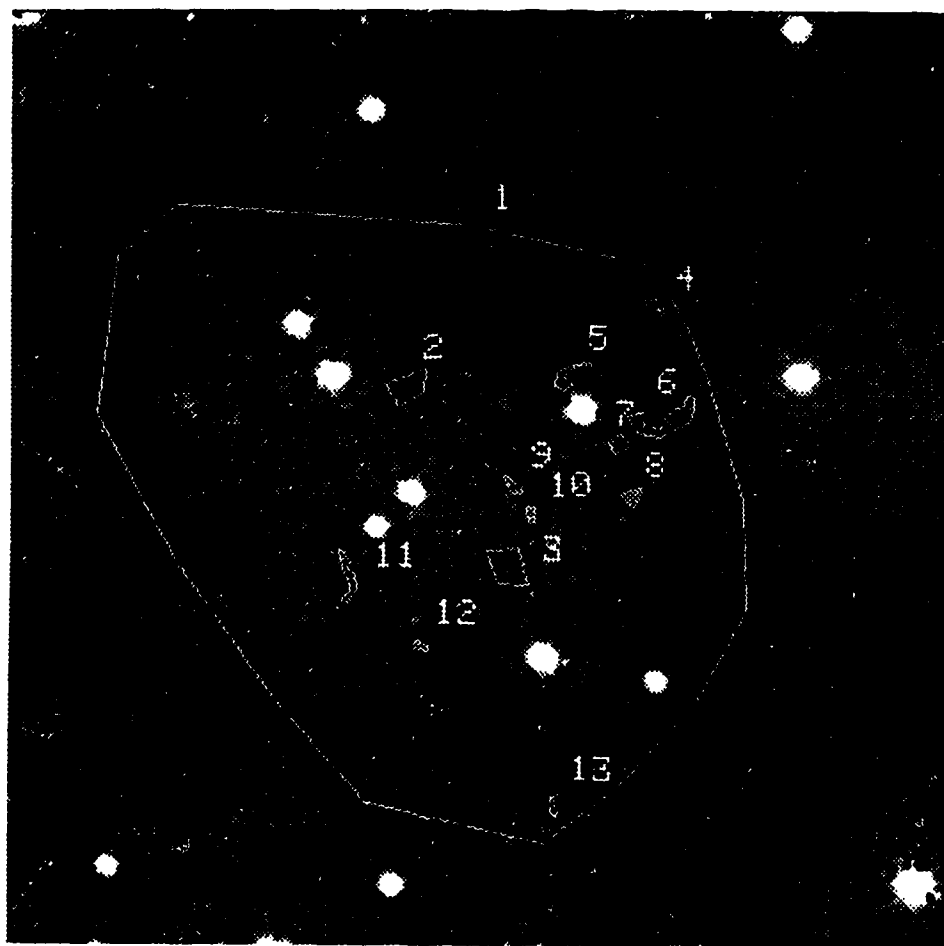


Fig. 17. An H_β filter image of CTB87 with the majority of stars removed. The outlined regions are those for which data are presented in Tables 4 and 5.



Fig. 18. An [OIII] filter image of CTB87 with the majority of stars removed. The outlined regions are those for which data are presented in Tables 4 and 5.

Table 4. Surface Brightness for Identified Regions.

Region	B Filter	V Filter	H β Filter	[OIII] Filter
		(mag/arcmin ²)		
1	14.90 \pm 0.01	14.26 \pm 0.08	16.29 \pm 0.23	15.48 \pm 0.05
2	14.04 \pm 0.03	13.99 \pm 0.05	16.12 \pm 0.26	15.34 \pm 0.18
3	14.48 \pm 0.05	13.79 \pm 0.13	15.86 \pm 0.12	14.80 \pm 0.05
4	14.33 \pm 0.08	13.87 \pm 0.12	16.01 \pm 0.11	14.99 \pm 0.08
5	—	14.69 \pm 0.13	16.49 \pm 0.23	15.44 \pm 0.03
6	15.44 \pm 0.14	14.47 \pm 0.20	16.71 \pm 0.08	15.89 \pm 0.16
7	—	14.36 \pm 0.11	16.71 \pm 0.15	15.47 \pm 0.29
8	13.96 \pm 0.08	13.07 \pm 0.06	15.41 \pm 0.24	14.35 \pm 0.11
9	—	13.48 \pm 0.05	15.83 \pm 0.06	15.04 \pm 0.20
10	14.33 \pm 0.06	13.09 \pm 0.10	15.41 \pm 0.16	14.36 \pm 0.11
11	—	14.04 \pm 0.06	16.90 \pm 0.34	15.57 \pm 0.01
12	—	13.84 \pm 0.13	16.02 \pm 0.11	14.87 \pm 0.14
13	—	13.83 \pm 0.08	16.08 \pm 0.10	15.14 \pm 0.09

Table 5. Signal to Noise Ratio for Identified Regions.

Region	B Filter	V Filter	H β Filter	[OIII] Filter
1	293.0	584.7	993.6	607.5
2	43.0	59.7	69.2	54.7
3	28.4	46.8	88.0	57.8
4	17.2	20.6	31.6	39.7
5	—	14.9	33.6	26.6
6	10.9	29.5	42.6	27.5
7	—	19.6	22.9	17.5
8	16.2	54.5	57.8	52.4
9	—	30.7	55.2	22.6
10	20.8	41.0	47.2	40.9
11	—	28.1	24.9	17.6
12	—	18.8	27.8	21.7
13	—	29.2	36.6	27.3

from the listed magnitudes by a colour index correction. The default reference magnitude for POLYPHOT is 26.000; the required reference magnitudes for matching observed and published values for H_β and $[OIII]$ filters were 23.016 and 21.708, respectively.

The V filter magnitudes were corrected by comparing apparent brightnesses of prominent field stars with values given in the Hubble Space Telescope Guide Star Catalogue version 3.0 on CD. None of the stars used for comparison included saturated or near-saturated pixels. A total of 13 stars were used; the reference magnitude determined was 21.301.

Magnitude values listed in Table 4 are averages of all images using the same filter. Uncertainty in magnitude is due to processing noise and photon statistics, or is the standard deviation of averaged values when this seemed a more reasonable estimate (usually when this was larger than the other noise sources; a likely cause of small variations between images is deviations between regions in different images).

Systematic error arises from the calibration. The magnitude values are calibrated by averages of known brightnesses of M57 (for B, H_β and $[OIII]$ filters) and HST Guide stars (for the V filter). This method usually introduces a small systematic error when the transformation equations between instrumental magnitudes and the standards used in reporting known magnitudes are not known. The significance of this effect is unknown, but it should not be too great (an extreme upper limit of about 0.40 mag is my estimate). B, H_β and $[OIII]$ magnitudes for M57 varied from image to image. Instrumental values in these filters were 16.118 ± 0.004 , 15.490 ± 0.007 and 14.233 ± 0.003 respectively. The B filter value in the literature was 9.84, essentially constant over a 20 year span [Kostyakova, 1992]. The consistency

of the magnitudes from image to image (for each filter) and the steadiness of M57 as an emitter indicate that 0.40 mag is a reasonable bound on the systematic error for these three filters. For the V filter, the HST Guide Star Catalogue listed a uniform uncertainty of 0.37 mag. Since the standard deviation of stellar magnitude differences between each image and the catalogue values was always significantly below this value, and image to image magnitude differences were typically below 0.04 mag, 0.40 mag is a reasonable bound for the V filter.

The values in Table 5. are signal to noise ratios for all the objects measured by POLYPHOT. They were derived according to the formula found in Newberry (1991):

$$S/N = (gain)Z_{obj} \left[(gain)Z_{obj} + n((gain)z_{sky,avg} + B^2)(1 + \frac{1}{n_{sky}}) \right]^{-1/2} \quad (10)$$

where Z_{obj} is the number of counts in ADU for an object, $z_{sky,avg}$ is the number of counts in ADU in a pixel of background sky, n is the number of pixels in the object, n_{sky} is the number of pixels used in background sky estimation and B is the base-level noise as defined for equation (5) with the exception that the overscan correction noise component is here the total processing noise in electrons. The relatively large S/N values for Region 1 are due to its large size and total signal with respect to the chosen background sky level. If most or all of the pixels in a region are roughly constant in intensity, the value of S/N varies almost linearly with size. Individual pixels in the various regions have S/N values from near 0 up to near 10. The table values are for the object as a whole.

The identified regions have the following characteristics:

Region 1 - The entire region exhibiting optical emission whose

boundaries roughly conform to the radio map extent of CTB87. All saturated star counts and counts from features not associated with the SNR, as judged by the author, are removed from the result. The variation of the region's location from image to image introduces some small error to the results: one image may have more non-emitting area within this region than another image. The differences are small when considering the large area of the SNR in comparison to any differences in size between images, though regions 2 and 3 may be more reliable estimates of surface brightness for CTB87. Magnitude is determined from counts above a background sky level.

- Region 2 - A region enclosed within diffuse emission towards the northeast end of CTB87. Magnitude is determined from counts above the same sky level as region 1.
- Region 3 - A region enclosed within diffuse emission towards the southwest end of CTB87. Magnitude is determined in a like manner to region 2. Region 3 is typically brighter than region 2.
- Region 4 - A region including part of an arc of emission located in the bulge of CTB87 towards the northwest. This arc appears to contain 3-5 stars, with nebulous strands between them. This region includes only filamentary emission. Magnitudes for this region and all remaining regions are determined by counts above a "sky" level calculated from nearby pixels. These values thus represent the brightnesses of supposed filaments above the level of diffuse emission from CTB87.
- Region 5 - A filamentary structure near a relatively bright star (9.94 ± 0.37 V mag. from the HST catalogue). The filament is thin and distinct.
- Region 6 - A region including most of an arc of emission located in the bulge of CTB87 towards the northwest. This arc opposes the arc of region 4: it is concave viewed from the north, while the other is concave viewed from the south. This arc may contain 1-2 stars in the southernmost part of it. Their light contributes to the brightness of this

region. These arcs may be distinct from CTB87 in origin — further study is required for a determination of their nature.

- Region 7 - This region contains a patch of emission which remains unresolvable into stellar profiles even at exposure times 10% longer than the usual maximum.
- Region 8 - A bright patch of emission which short exposures leave unresolved. Maximal exposure times identify slightly brighter portions which conform enough to stellar full-width-half-maximum profiles to be identified by IRAF Tasks as stars. This identification, however, is not definite. The patch is not obviously resolvable into distinct objects for exposure times up to the longest used.
- Region 9 - A filament of emission which possibly contains distinct objects. The proximity of this region to the central portion of CTB87 and the “smearing” of emission between bright spots lead to its inclusion in this list.
- Region 10 - A region similar in nature to region 9. One nearby bright object at the southwest point was excluded. Its separation from the rest of the region indicated that it is likely to be a star.
- Region 11 - An extended filamentary arc in the best images, this region becomes a chain of emission patches in some images where the dimmer links in the chain are indistinct. Roughly two-thirds of the distance from northeast to southwest along the filament, lies a relatively bright star (B: 13.959 ± 0.004 ; V: 13.375 ± 0.033 ; H_β : 16.079 ± 0.019 ; [OIII]: 14.907 ± 0.029). In the middle of the filament another star (about 2 mag fainter in each filter) is situated. The removal of either star by IRAF Tasks does not affect the appearance of the filaments, the extra emission across the star from the filament is roughly constant.
- Region 12 - An isolated region. Its smeared appearance requires a much longer exposure to deny its filamentary nature.
- Region 13 - A curved filament, likely containing at least one star.

In general, CTB87 appears as an elliptical region of diffuse emission lying

at a eastward angle of roughly 30° from a line of right ascension. There is a slight bulge towards the northwest containing two filamentary arcs. Two arcs and several patches are highlighted against the main elliptical portion of the SNR.

In B filter light, the nebulosity is extremely faint, though key filaments do show up. The diffuse emission does not rise dramatically from the background. In V filter light, CTB87 seems to be attached to a large region of nebulosity to the southwest. The nebular brightness is peaked in the CTB87 region, falls off slightly to the southwest, and then rises again. In other directions, emission falls off rapidly.

The line filters provide the clearest view of the SNR. In H_β light, the emission nebula is distinct as light falls off rapidly from a bright central mass. The filaments are prominent. In [OIII] light, CTB87 is not quite as distinct as it is in H_β , though the flux through this filter is larger. The diffuse emission still conforms to expectations, with a central bright mass that falls off rapidly near the edges. The filaments are distinctly present, though with expected slight differences from each of the other filters.

Although neither Visual or Red Palomar Sky Survey plates show evidence of nebulosity, the images presented in *An Emission-Line Survey of the Milky Way* [Parker, Gull and Kirshner, 1979] reveal nearby emission. The survey was completed in narrow bands about 4225\AA (CaI), 4864\AA (H_β), 5010\AA (near OIII), 6570\AA (H_α) and 6736\AA (SII), and is composed of 7° fields. Two fields ($l = 78^\circ, b = 0^\circ; l = 73^\circ, b = 0^\circ$) overlapped the CTB87 region, though the SNR was near the edge of each field. At 4225\AA and 4864\AA , CTB87 was just outside the periphery of the large region of nebulosity to the west. At 5010\AA , emission is roughly uniform across the CTB87 region. At the longer

wavelengths, CTB87 lies within an area of strong emission. The large size of these fields in relation to images taken for the present work makes a detailed comparison of CTB87 features untenable. However, the survey fields do not show the concentration of emission evident in the new H_β and [OIII] images.

In all CTB87 images, there are nearby emission patches. Prominent patches lie to the west, southwest and south-southwest that are all within 10 arcmin of the SNR. An early conjecture that perhaps the observed nebulosity was merely light from bright stars that was diffracted onto surrounding areas of the chip is denied by the shape and location of emission patches. While within CTB87 several bright stars lie on top of the central bright emission, other stars of similar magnitude outside the region do not possess light envelopes. The conclusion is thus that the nearby emission is real (fortunately), and might be linked to the nearby nebulosity shown in Parker, Gull and Kirshner (1979).

The B, V, H_β and [OIII] filters used are not entirely distinct in their spectral coverage. The H_β and [OIII] passbands are both included within the V filter coverage. The observed magnitudes indicate that about 15% of V emission is in the H_β band, and 32% is in the [OIII] band. Line emission seems to be the most significant contribution to emission in the optical domain, though thermal emission should play a larger role near the infrared end. The B and V filters are to be distinct in spectral coverage. The relatively low brightness of the nebula in B images confirms that neither H_β nor [OIII] passbands are included.

The emission observed from CTB87 in the present work is low. One must assume a nebular size to speak of a limiting surface brightness for detection; the character of the emission would also affect detectability (CTB87's ap-

pearance is such that without knowledge of the presence of the SNR from radio information, it would not be identified optically). A better idea of the depth available from the Devon Observatory CCD system lies in checking stellar limiting magnitudes.

The star identified in Figure 10 (pg.33) as "LIMIT" is that used to test the magnitude limits of the CCD chip in each filter. The star's apparent magnitudes (instrumental corrected for the proper magnitude zero point) are 15.891 ± 0.013 in B, 15.007 ± 0.007 in V, 17.626 ± 0.008 in H_β and 16.509 ± 0.006 in OIII light. Assuming that the limiting magnitude is specified by S/N of 5, equation (10) and the definition of the magnitude scale allow one to calculate the limit, using the star "LIMIT" as a reference. The limiting magnitudes for each filter are approximately: 19.89 for a 450 second B filter exposure, 20.01 for a 180 second V filter exposure, 22.57 for a 500 second H_β filter exposure, 21.39 for a 530 second [OIII] exposure.

3.5 MOSAIC CONSTRUCTION

Each observing session produced a set of fields covering CTB87 and its surroundings. The extent of this map was approximately 25×25 arcmin. In addition to the central field, which included the entirety of the SNR's radio extent, four images centred roughly at the corners of the original image comprised the set. When combined in a mosaic, these images provide a wide-angle view of CTB87.

The mosaic components were initially displayed singly, to orient them relative to one another using common stars. The Task IRMOSAIC then created a rectangular template containing all component images. The next step was the creation of a file containing coordinate pairs for stars common to

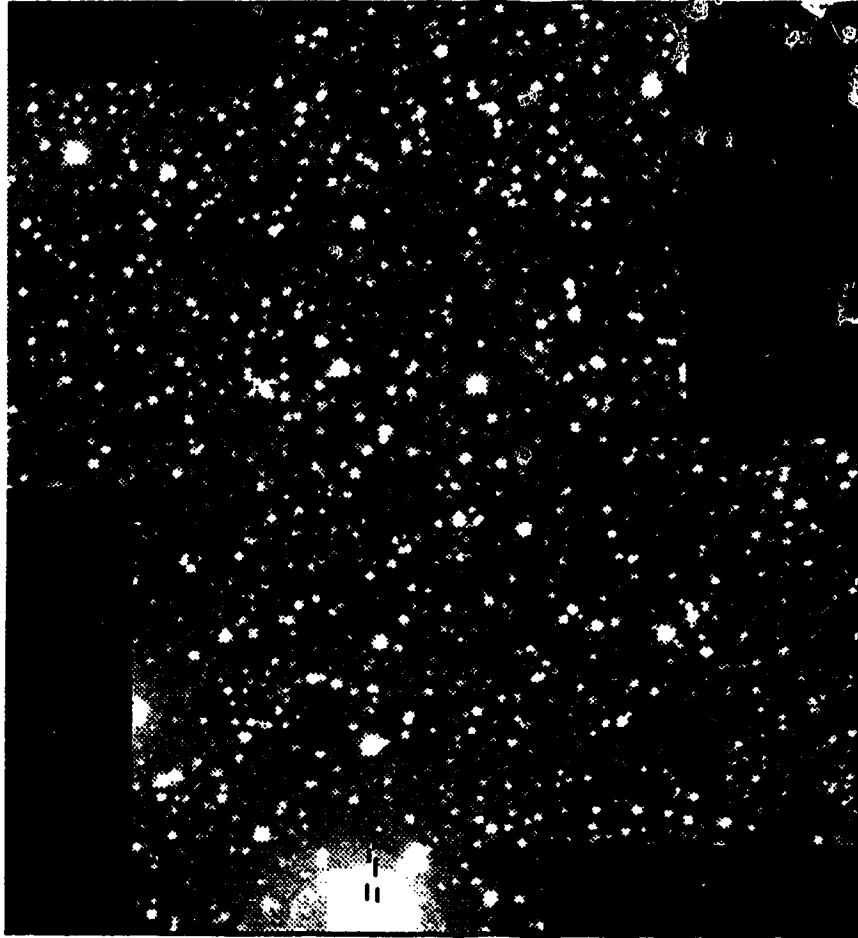


Fig. 19. A B filter mosaic of the CTB87 region.

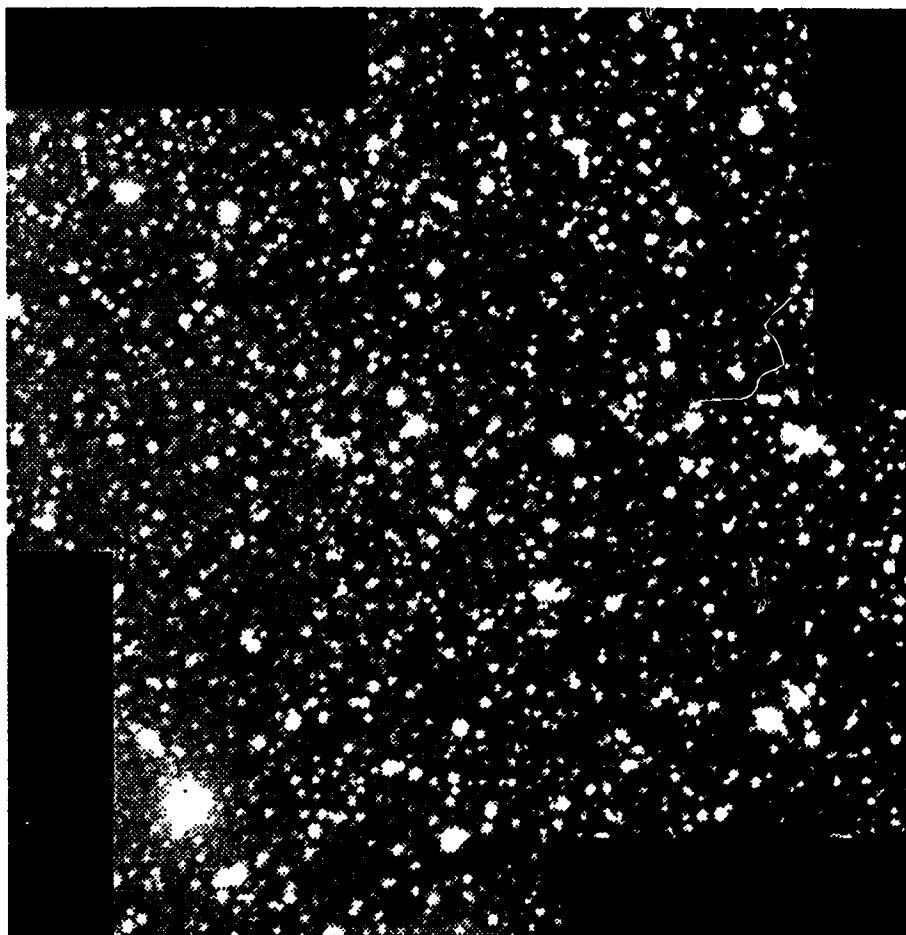


Fig. 20. A V filter mosaic of the CTB87 region.

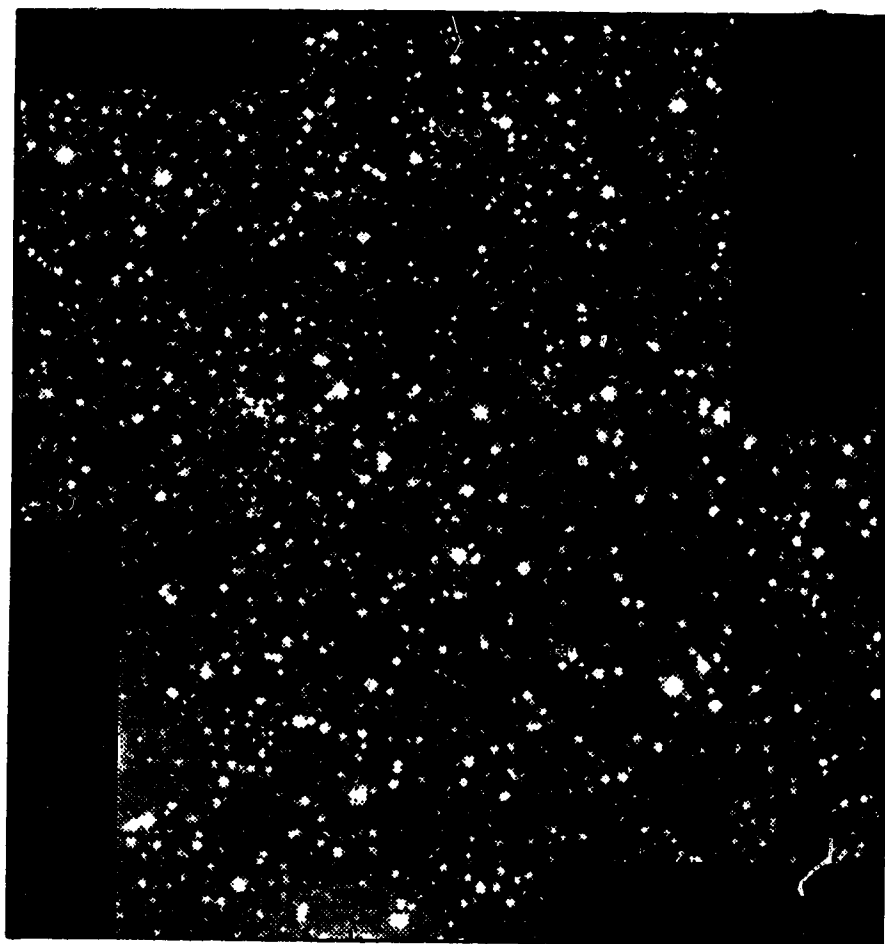


Fig. 21. An H_{β} filter mosaic of the CTB87 region.

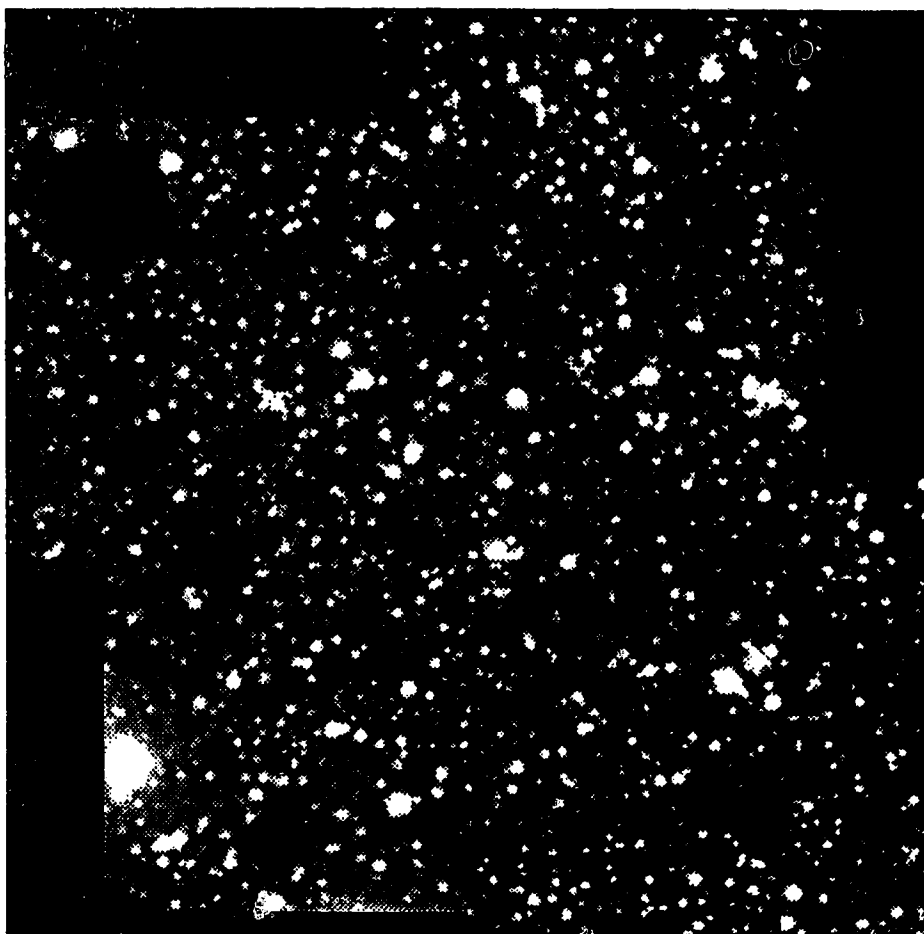


Fig. 22. An [OIII] filter mosaic of the CTB87 region.

pairs of component images within the template. This file and the template image were input to IRMATCH2D. This Task copies component images individually into the final image. Each component is scaled by the mode of the overlapping region, and clipped to a specified size before integration into the mosaic. Figures 19 through 22 show examples for each filter. For further details on the creation of mosaic images, see Appendix D.

In each image, emission is fairly distinct in the CTB87 area. Other emission regions in V, H_{β} and [OIII] light may appear to cast doubt on the identification of the observed emission with CTB87, yet the position in each filter of this emission within the radio outlines of the SNR is persuasive (see Figure 23 in Chapter 4). In my opinion, this coincidence of location, when coupled with the fact that [OIII] emission is a strong indicator of SNR, demonstrates that at least a significant portion of the signal reported in Table 4 is due to CTB87.

CHAPTER FOUR: CONCLUSIONS

The present work provides an illustration of the use of the Devon Astronomical Observatory in acquiring optical images of radio-identified objects, specifically the first optical detection of supernova remnant CTB87.

Comparison of important CCD chip characteristics was made with data from previous photometric work with the Devon telescope [Steinbring, 1995]. In the interim between observing sessions relevant to the photometric work and this work, the CCD camera was serviced by the retailer, SpectraSource Instruments Incorporated. The chip characteristics that underwent a significant change were gain, readout noise, dark current and dynamic range. Gain dropped to $4.6\text{ e}^-/\text{ADU}$ from $4.9\text{ e}^-/\text{ADU}$; readout noise was vastly improved from 79 e^- to between 21 and 29 e^- ; dark current was greatly reduced from 50 ADU/pixel/s ($245\text{ e}^-/\text{pixel/s}$) to $\sim 0.33\text{ ADU/pixel/s}$ ($\sim 1.5\text{ e}^-/\text{pixel/s}$); dynamic range of the CCD increased by $\sim 4.5\text{ dB}$ (primarily due to the readout noise reduction).

The limiting magnitude in the V filter was reported to be ~ 17 th magnitude for a 180 second exposure [Steinbring, 1995]. Using the same criterion for locating the limiting magnitude, this has been improved in the interim to ~ 20 th magnitude. The B, H_β and [OIII] limiting magnitudes are ~ 20 th magnitude for 450 seconds, ~ 22.6 th magnitude for 500 seconds and ~ 21.4 th magnitude for 530 seconds, respectively.

I have accomplished the first optical identification of the supernova remnant CTB87. The emission has an elliptical shape of anisotropic intensity across the nebula (it is centrally peaked). I find surface brightness values

of 14.04 mag/arcmin² in B, 13.79 mag/arcmin² in V, 15.86 mag/arcmin² in H β and 14.80 mag/arcmin² in [OIII] lights near the peak (H β and [OIII] values calibrated to the V magnitude scale). It is significantly fainter than the calibration object M57 (whose surface brightnesses in B, H β and [OIII] are 12.89, 13.35 and 10.79 mag/arcmin² respectively) and also M1 (Crab Nebula) (surface brightness in V \sim 10 mag/arcmin²), which was the first (brightest) plerion to be classified. This identification of CTB87 is encouraging in that it cultivates hope that other faint radio SNRs may be available for study at optical wavelengths, even though the distance to CTB87 may be much smaller than HI absorption studies indicate.

The central diffuse emission of CTB87 is accompanied by a number of filaments and bright patches. The extent of the optical emission conforms roughly to the extent of radio emission, and encompasses the region of x-ray emission from CTB87, as shown in Figure 23. Further detailed spectral investigation¹¹ will result, I hope, confirming the identity of this optical emission as originating with CTB87.

¹¹ Spectra of individual filaments would identify any chains of stars which were mistaken for nebula components. Analysis of the individual line profiles from filament and diffuse emission would provide information on the dynamics of the emitter. Further line emission fluxes may be measured, and comparison made with known line ratios of similar SNRs to confirm its nature.

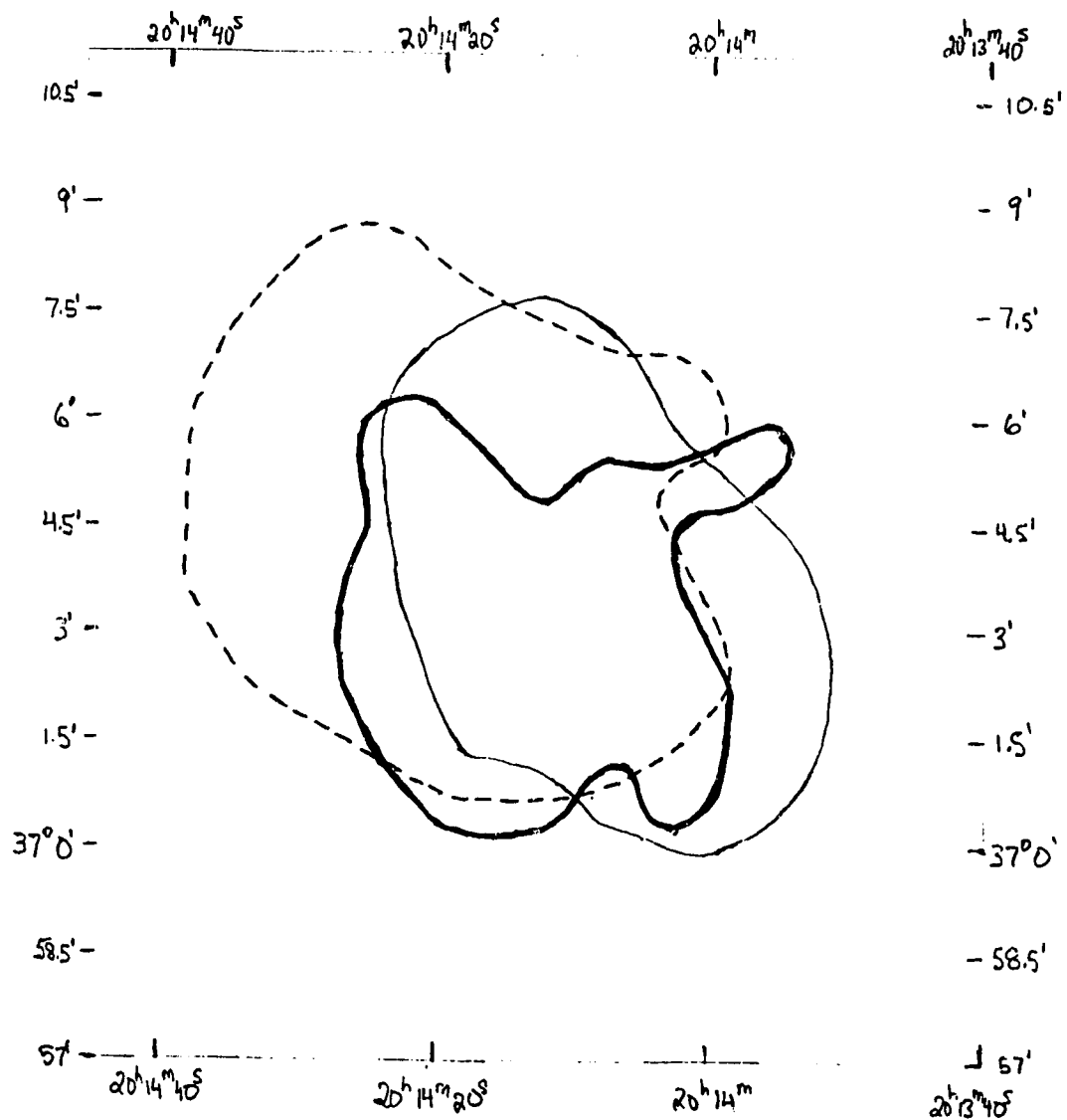


Fig. 23. CTB87 emission perimeters in radio (line), optical (dashed line) and x-ray (heavy line) energy domains plotted against the celestial sphere. The radio and x-ray perimeters are taken from Cho, Kim and Fukui (1994). The optical perimeter is from a typical $H\beta$ image.

REFERENCES

- Arp, A., Stenholm, B., Tytenda, R. and Raytchev B. The Absolute $H\beta$ Fluxes for Galactic Planetary Nebulae, *Astron. Astrophys. Suppl. Ser.* 90, pp 89-101. 1991.
- Asaoka, Ikuko and Koyama, Katsuji. Do All the Crab-Like Supernova Remnants Have an X-Ray Photon Index Near a Value of 2?, *Publ. Astron. Soc. Japan* 42, pp 625-632. 1990.
- Bartel, Norbert (Ed.). *Supernovae as Distance Indicators*. Springer-Verlag, Berlin. 1985
- Cho, Se-Hyung, Kim, K.T. and Fukui, Y. CO Study of the Giant Molecular Cloud Towards Supernova Remnant CTB87, *Astron. J.* 108(2), pp 634-638. 1994.
- Clark, D.H. and Caswell, J.L. A Study of Galactic Supernova Remnants, Based on Molonglo-Parkes Observational Data, *Mon. Not. R. astr. Soc.* 174, pp 267-305. 1976.
- Cosmovici, Cristiano Batalli (Ed.). *Supernovae and Supernova Remnants*. D. Reidel Publishing Company, Dordrecht. 1973.
- Crawford, D.L. and Mander, Jeannette. Standard Stars for Photoelectric $H\beta$ Photometry, *Astron. J.* 71(2), pp 114-118. 1966.
- Duin, R.M., Israel, F.P., Dickel, J.R. and Seaquist, E.R. The Nonthermal Radio Sources at $l = 74.9^\circ$ and $b = +1.2^\circ$, *Astron. Astrophys.* 38, pp 461-465. 1975.
- Fesen, Robert A., Gull, Theodore R. and Ketelsen, Dean A. Deep [OIII] Interference Filter Imagery of the Supernova Remnants G65.3+5.7, G126.2+1.6, CTA1 and VRO 42.05.01, *Astrophys. J. Suppl. Ser.* 51, pp 337-344. 1983.
- Fesen, Robert A., Blair, William P. and Kirshner, Robert P. Optical Emission-Line Properties of Evolved Galactic Supernova Remnants, *Astrophys. J.* 292, pp 29-48. 1985.
- Frail, D.A., Kassim, N.E., Cornwell, T.J. and Goss, W.M. Does the Crab Have a Shell?, *Astrophys. J.* 454, pp L129-L132. 1995.
- Geldzahler, B.J. Very High Resolution Observations of Compact Sources in the Direction of Supernova Remnants: G74.87+1.22, *Astrophys. J.* 286, pp 284-288. 1984.
- Gorham, Peter W., Ray, Paul S., Anderson, Stuart B., Kulkarni, Shrinivas R. and Prince, Thomas A. A Pulsar Survey of 18 Supernova Remnants, *Astrophys. J.* 458, pp 257-264. 1996.
- Green, D.A. A Revised Reference Catalogue of Galactic Supernova Remnants, *Astrophysics and Space Science* 148, pp 3-74. 1988.

- Green, D.A. **Limitations on Statistical Studies of Galactic Supernova Remnants By Observational Selection Effects**, *Publ. Astron. Soc. Pac.* 103, pp 209-220. 1991.
- Green, D.A. **The Spectral Turnover of the "Filled-Center" Supernova Remnant 3C 58: Implications for When Acceleration Occurs**, *Astrophys. J. Suppl. Ser.* 90, pp 817-821. 1994.
- Green, D.A. and Gull, S.F. **Observations of H I Absorption Towards G74.9+1.2**, *Mon. Not. R. astr. Soc.* 237, pp 555-559. 1989.
- Gull, Theodore R., Kirshner, Robert P. and Parker, Robert A.R. **A New Optical Supernova Remnant in Cygnus**, *Astrophys. J.* 215, pp L69-L70, 1977.
- Hayes, D.S., Pasinetti, L.E. and Philip, A.G. Davis. (Eds.). *Calibration of Fundamental Stellar Quantities*. D. Reidel Publishing Company, Dordrecht. 1984.
- Kazés I. and Caswell, J.L. **Distance Estimates for the SNR G74.9+1.2 and a Nearby Point Source**, *Astron. Astrophys.* 58, pp 449-450. 1977.
- Kitchin, C.R. *STARS, NEBULAE AND THE INTERSTELLAR MEDIUM Observational Physics and Astrophysics*. Adam Hilger, Bristol. 1987.
- Kjeldsen, Hans and Frandsen, Søren. **High-Precision Time-Resolved CCD Photometry**, *Publ. Astron. Soc. Pac.* 104, pp 413-434, 1992.
- Koo, Bon-Chul and Heiles, Carl. **A Survey of H I 21 Centimeter Emission Lines Toward Supernova Remnants**, *Astrophys. J.* 382, pp 204-222. 1991.
- Kostyakova, E.B. **Physical Variability of Planetary Nebulae: Mean Photoelectric *UBV* magnitudes of Seven Objects (1968-1988)**, *Sov. Astron. Lett.* 16(6), pp 465-469. 1990.
- Kostyakova, E.B. **The Mean Integrated *UBV* magnitudes of Seven Planetary Nebulae From 1968 to 1988**, *Sov. Astron. Lett.* 18(5), pp 324-326. 1992.
- Kovalenko, A.V., Pynzar, A.V. and Udaltsov, V.A. **Observations of Supernova Remnants at Pushchino: Compiled Spectra of Supernova Remnants**, *Astronomy Reports* 38(1), pp 78-94. 1994. (1994a)
- Kovalenko, A.V., Pynzar, A.V. and Udaltsov, V.A. **Observations of Supernova Remnants at Pushchino: Catalog of Flux Densities at Meter Wavelengths**, *Astronomy Reports* 38(1), pp 95-103. 1994. (1994b)
- Kundt, Wolfgang (Ed.). *Supernova Shells and Their Birth Events*. Springer-Verlag, Berlin. 1988.
- Lame, Nancy Joanne and Pogge, Richard W. **Imaging Spectrophotometry of the Planetary Nebula NGC 6720 (The Ring Nebula)**, *Astron. J.* 108(5), pp 1860-1871. 1994.
- Lang, Kenneth R. *ASTROPHYSICAL FORMULAE A Compendium for the Physicist and Astrophysicist*. Springer-Verlag, Berlin. 1980.

- Leahy, D.A. *Einstein X-Ray Observations of the Supernova Remnant HB21*, *Mon. Not. R. astr. Soc.* **228**, pp 907-913. 1987.
- Mathewson, D.S., Ford, V.L., Dopita, M.A., Tuohy, I.R., Long, K.S. and Helfand, D.J. *Supernova Remnants in the Magellanic Clouds*, *Astrophys. J. Suppl.* **51**, pp 345-355. 1983. (1983a)
- Mathewson, D.S., Ford, V.L., Dopita, M.A., Tuohy, I.R., Long, K.S. and Helfand, D.J. , *Supernova Remnants and Their X-Ray Emission*, J. Danziger and P. Gorenstein (Eds.), pp 541-549. D. Reidel Publishing Company, Dordrecht. 1983. (1983b)
- Mathewson, D.S., Ford, V.L., Dopita, M.A., Tuohy, I.R., Mills, B.Y. and Turtle, A.J. *Supernova Remnants in the Magellanic Clouds*, *Astrophys. J. Suppl.* **55**, pp 189-210. 1984.
- Marschall, Laurence A. *The Supernova Story*. Plenum Press, New York, 1988.
- Meyerott, Roland and Gillespie, George H. (Eds.). *Supernovae Spectra*. American Institute of Physics, New York. 1980.
- Morsi, H.W. and Reich, W. **32 GHz Radio Continua Observations of Four Plerionic Supernova Remnant**, *Astron. Astrophys. Suppl. Ser.* **69**, pp 533-540. 1987.
- Newberry, Michael V. **Signal-To-Noise Considerations for Sky-Subtracted CCD Data**, *Publ. Astron. Soc. Pac.* **103**, pp 122-130. 1991.
- Odenwald, Sten F. and Schwartz, Phil R. **An IRAS Survey of Star-Forming Regions Toward Cygnus**, *Astrophys. J.* **405**, pp 706-719. 1993.
- Parker, R.A.R., Gull, T.R. and Kirshner, R.P. *An Emission Line Survey of the Milky Way*. NASA-SP 434, 1979.
- Pineault, Serge and Chastenay, Pierre. **Radio Continuum Observations of a Galactic Field Centred on the Supernova Remnant G73.9+0.9**, *Mon. Not. R. astr. Soc.* **246**, pp 169-182. 1990.
- Roger, R.S. and Landecker, T.L. *Supernova Remnants and the Interstellar Medium*. Cambridge University Press, Cambridge. 1987.
- Rosado, M. **Kinematics of the Supernova Remnant G65.2+5.7 in Cygnus**, *Astrophys. J.* **250**, pp 222-226. 1981.
- Salter, C.J., Reynolds, S.P., Hogg, D.E., Payne, J.M. and Rhodes, P.J. **84 GigaHertz Observations of Five Crab-Like Supernova Remnants**, *Astrophys. J.* **338**, pp 171-177. 1989.
- Schramm, David N. *Supernovae*. D. Reidel Publishing Company, Dordrecht. 1976.
- Seward, Frederick D. **The Crab-Like Supernova Remnants**, *Space Sci. Rev.* **49**, pp 385-423. 1989.

- Seward, Frederick D. *Einstein Observations of Galactic Supernova Remnants*, *Astrophys. J. Suppl. Ser.* **73**, pp 781-819. 1990.
- Seward, Frederick D. and Wang, Zhen-Ru. *Pulsars, X-Rays Synchrotron Nebulae and Guest Stars*, *Astrophys. J.* **332**, pp 199-205. 1988.
- Sitnik, T.G., Pravdikova, V.V. and Mel'nikov, V.V. *High-Velocity Flows of Ionized Hydrogen in the Southern Part of the Cyg I Supershell*, *Astronomy Letters* **21**(1), pp 107-115. 1995.
- Steinbring, Eric. *The Devon Observatory CCD Imaging System and its Application to Photometry of the Ellipsoidal Variable HR 4646*. University of Alberta, Edmonton. 1995.
- Taylor, A.R., Wallace, B.J. and Goss, W.M. *New Galactic Plane Supernova Remnants*, *Astron. J.* **103**(3), pp 931-942. 1992.
- Wallace, B.J., Landecker, T.L. and Taylor, A.R. *H_I Voids Around Filled-Center Supernova Remnants*, *Astron. Astrophys.* **286**, pp 565-578. 1994.
- van Gorkom, J.H., Goss, W.M., Seaquist, E.R. and Gilmore, W.S. *H_I Absorption Distances to Four Point Sources Near Supernova Remnants*, *Mon. Not. R. astr. Soc.* **198**, pp 757-765. 1982.
- Wang, Z.-R., Lin, J.Y., Gorenstein, P. and Zombeck, M.V. , *Highlights Astron.* **7**, pp 583-1986.
- Weiler, K.W. and Panagia, N. *Vela X and the Evolution of Plerions*, *Astron. Astrophys.* **90**, pp 269-282. 1980.
- Weiler, K.W. and Shaver, P.A. *Total Intensity and Polarization Structure of the Supernova Remnant G74.9+1.2 at $\lambda\lambda$ 6, 21, 49 Centimeters*, *Astron. Astrophys.* **70**, pp 389-397. 1978.
- Weiler, K.W. and Sramek, Richard A. *Supernovae and Supernova Remnants*, *Ann. Rev. Astron. Astrophys.* **26**, pp 295-341. 1988.
- Wendker, H.J., Higgs, L.A. and Landecker, T.L. *THE CYGNUS X REGION XVIII. A Detailed Investigation of Radio-Continuum Structure on Large and Small Scales*, *Astron. Astrophys.* **241**, pp 551-580. 1991.
- Wheeler, J. Craig (Ed.). *SN I*. The University of Texas at Austin and McDonald Observatory, Austin. 1980.
- Willis, A.G. *Observations of Galactic Supernova Remnants at 1.7 and 2.7 GHz*, *Astron. Astrophys.* **26**, pp 237-255. 1973.
- Wilson, A.S. *X-Rays From G74.9+1.2: An Elderly Crab Nebula?*, *Astrophys. J.* **241**, pp L19-L22. 1980.

APPENDICES

GENERAL NOTE: These procedures are written for the Linux version of IRAF. For the older Unix version, see the author about Tasks that do not appear. The procedures are generally the same though.

APPENDIX A:

IRAF Reduction Procedures

(for an image with header file imname.imh)

This appendix details the procedures for processing raw data frames into frames which may be used in quantitative analysis.

Initialisation:

- open a working window (`/usr/openwin/demo/xterm &` on STELLAR, `xgterm &` on GALAXY)
- open an “SAOimage” window (`/usr/local/bin/saoimage &` when on STELLAR, `saoimage &` on GALAXY)
- select the working window, “cd” to your IRAF directory (where your `login.cl` resides), and type “cl” to start IRAF from this window

1. Group data images based on time and/or sky position

Grouping is handy for large numbers of images, and allows greater accuracy if calibration images (darks, biases and flats) are taken for each group. Usually, the increase in accuracy is minimal, since the calibration images **should not** experience significant changes in the course of an observing run, but uncertainties are reduced. For each group, a file should be created containing the image names.

2. Group calibration images and set combination parameters (`noao` → `imred` → `ccdred`)

If calibration images are taken for each group of observations, they should be the only ones used to reduce the corresponding group. It is advisable to combine many exposures to produce a master image (ie. take several bias (zero) exposures and form an **averaged** bias (zero) image). The form of combination is here taken to be synonymous with averaging (the average of intensity values from each frame is determined pixel-by-pixel). This can amount to a significant reduction of magnitude uncertainties (better signal-to-noise ratios). One may use either the Task corresponding to a particular image type (**zerocombine**, **darkcombine** or **flatcombine**), or the generic **combine** Task. If only one of each type of calibration frame is exposed per group, then the raw calibration image can be used directly in **ccdproc** without combining it with any others. This is **not** recommended.

The header files for calibration images should first be edited to reduce errors. All images are assumed to be stored as real numbers on conversion to IRAF format.

hedit *inputlist* *imagetype* *zero*

zerocombine *inputlist*

darkcombine *inputlist*

flatcombine *inputlist*

combine *inputlist* *outimage*

inputlist is the list of input calibration images of the relevant type (it is **not** the same for each of these Tasks, it refers only to the group list for the particular image type specified)

zero is the *imagetype* (one of zero, dark, flat or object)

For **hedit**, ensure that the parameter *add* is set to “yes”, and *delete* to “no” (check with **eparam hedit**). Make sure the images are labelled with the appropriate type. The default parameter values for the remaining Tasks are readily usable except for

output, *reject*, *ccdtype*, *process* and *scale*. The *output* parameter is the name of the combined image. The effect of the default value of *reject* may be improved in most cases by replacing it with “*avsigclip*”. *ccdtype* is the type of image being combined (the same as the value of the header keyword *imagetype* which was set by *hedit*). The *process* parameter tells the Task whether or not it should use **ccdproc** on the images before combining them (**ccdproc** is explained in step 3, where the settings are specified for the combining Tasks). This should be set to “yes”. The *scale* parameter should be set to “none” for bias frames, and “exposure” for darks and flats.

When using the **combine** Task, the variables *ccdtype*, *combine*, *reject* and *scale* may be changed dependent upon the image type (including object) being combined. Use **help combine** to investigate proper settings.

NB: Before running **flatcombine**, remove from your list any images that have significant pixel regions that are oversaturated. Also set *scale* to “mean” for sky flats.

3 Process the images

Before running each of the combining Tasks, edit the parameter file for **ccdproc**. Set *ccdtype* to null (type “ ”), and *zerocor*, *darkcor* and *flatcor* to “no”. Set *biassec* to a representative section of the overscan region (if it’s being used, otherwise set *overscan* to “no”). Set *trimsec* to the area of the image containing data (eg. [1:512,1:512]). Then run **zerocombine**. Afterwards, set the **ccdproc** parameters *zerocor* and *zero* to “yes” and the value of **zerocombine** parameter *output*, respectively. Then **darkcombine** may be used. Follow the same procedure for *darkcor* and *dark* before running **flatcombine**. Also before **flatcombine**, replace any oversaturated pixels by a reasonable intensity value (for the HPC-1 camera at Devon, these pixels will have a value below -32760 in a raw frame and should be replaced by +32768; use the command: **imrep inputlist 32768**

lower=INDEF upper=-32760). Then **ccdproc** may be used on the object fields.

Running **ccdproc** separately on each group of field images will complete the processing. For simple and successful execution of this Task, there are two options. For each group of field images, the file containing the list is used as input and one must change the parameter file of **ccdproc** by specifying the “zero”, “dark” and “flat” files to use for this group. This requires one to edit the parameters after each group. Alternatively, if the CCD camera includes the image type (zero, dark, flat or object) in the header files for each image, then the group calibration image names should be included in the file containing the group list before running **ccdproc** (NB: Bias frames should be specified as type “zero” for IRAF). In this case, the *zero*, *dark* and *flat* parameters must be left empty in the **ccdproc** parameter file (type “ ” ” in the appropriate row), and the *ccdtype* parameter should be set to “object”.

NB: Oversaturated pixels in the field images **MUST** be replaced before processing. Use **imreplace** as above before **ccdproc**, but remember to specify only the data region of the image (do not include the overscan) in the inputlist. One may now run **ccdproc**:

ccdproc @grpname

grpname is the file containing the group of images to be processed. The “@” symbol indicates that the image names are stored inside this file.

APPENDIX B:

IRAF Photometry Procedures

(for an image with header file imname.imh)

This appendix contains detailed procedures for acquiring instrumental magnitudes for both crowded and uncrowded field images. Uncrowded fields are those in which the stars of interest are many magnitudes brighter than any within 4 full-width-half-maximum (FWHM) units of the stars' centres. Photometry is then limited to the specified stars. Other fields are crowded.

Initialisation:

- open a working window (`/usr/openwin/demo/xterm &` on STELLAR, `xgterm &` on GALAXY)
- open an "SAOimage" window (`/usr/local/bin/saoimage &` when on STELLAR, `saoimage &` on GALAXY)
- select the working window, "cd" to your IRAF directory (where your `login.cl` resides), and type "cl" to start IRAF from this window

1. Preprocess image (`noao` → `imred` → `ccdred`).

- see *IRAF Reduction Procedures* (Appendix A)

2. Display image (`images` → `tv`).

`display imname 1`

imname is the image name

1 is the frame number (from 1-4)

3. Determine image parameters.

`imexamine`

(for image FWHM)

- select the SAOimage window
- use cursor to select a typical star (centre cursor on star)
- press "r" to get a radial intensity plot

- repeat for other stars and record a representative FWHM for stars in the image
- record the radius at which wings of the brightest stars (that aren't saturated) disappear into the sky background (the axes of the radial plot may be reset by typing **rimexam** before entering **imexamine**)
- press "q" to exit

imstatistics *imname*[*x1:x2,y1:y2*] (for sky values)

- find a region free of stars, bounded by the coordinate set *x1*, *x2*, *y1*, *y2*
- record the sky brightness (mean) and fluctuations (standard deviation)

The *fw hm p s f* parameter is key for crowded field photometry. The values of sky brightness and deviations are determined as a default in the case of unusual apertures (shapes for objects). The deviation is also used to set the threshold for star detection used by **daofind** (explained in step 5).

4. Edit parameter files (**digiphot** → **daophot**).

datapars

- set *fw hm p s f* to measured stellar FWHM
- set *sigma* to background standard deviation
- set *threshold* to 5 x *sigma*
- set *ccdread* and *gain*, or *readnoise* and *epadu*
(*ccdread* and *gain* are header keywords, *readnoise* and *epadu* are numerical values in e^- 's and e^-/ADU)

photpars

- set aperture radius/radii to a value of 3-4 times *fw hm p s f* for uncrowded fields whose interesting stars are without companions, or to *fw hm p s f* otherwise; multiple apertures may be specified for each star, separated by blanks or commas

- if the correct zero point to the magnitude scale for the appropriate filter is known, *zmag* should be set

centerpars

- set *algorithm* to: “none” (when **phot** is run as a batch job), “centroid” or “gaussian” (when **phot** is run interactively)

fitskypars

- set *skyvalue* to sky brightness mean
- set *annulus* (inner radius of sky determination annulus) to just larger than the radius of wing vanishing determined from **imexamine**
- set *dannulus* (width of sky annulus; 10 is usually sufficient)

daopars

- specify variable or constant *psf* (*varpsf* = “yes” or “no”); first and second order variations across an image are calculable, but the initial use for each image should be with a constant point-spread-function (*psf*); when *varpsf* = “yes”, set *varorder* to “1” or “2”
- set *psfrad* to a value slightly larger than the radius of the largest stellar profile
- set *fitrad* to stellar FWHM
- set *sannulus* to the value of *annulus* from **fitskypars**
- set *wsannulus* to the **fitskypars** value of *dannulus*
- set *maxgroup* to maximum number of stars in any group to be examined
- set *maxnstar* to a value known to be larger than the number of stars in the image

5. Create a list of stars in the image and mark them.

daofind *imname* *daoffnm*

daoffnm is the output file for star coordinates

The user will then be prompted for *fwhmpsf* and *threshold*. Since the parameter files have been changed, the default values should be those entered. One need only hit <return>.

tvmark 1 daoffnm

1 is the frame number of the image
- colours and symbols used by tvmark may be changed (**eparam tvmark**) and are listed in the tvmark helpfile (**help tvmark**)

If there are obvious stars that have been missed, they may be appended to the file *daoffnm* (only coordinates and an ID number need be entered). If fainter stars are all missed, then *threshold* must be reduced.

6. Create a list of aperture magnitudes (rough values).

If only a small fraction of the stars in the image are of interest, then the file *daoffnm* should be edited to remove all **BUT** the important stars **AND** a region of stars surrounding them. If the field is crowded and the stars of interest have NO companions, then the surrounding stars may also be removed from the list. This should be done before running **phot**, to reduce runtimes in the later steps. The number of stars left in the *daoffnm* file must be sufficient to produce a good psf for a crowded field.

phot imname daoffnm photflnm

photflnm is the output file for aperture magnitudes

The user will then be prompted for *calgorithm*, *salgorithm*, *annulus*, *dannulus*, *sigma*, *apertures*, *datamax* and *datamin*. All default values should be correct, though *datamax* and *datamin* should be examined. If no important star is supersaturated, then *datamax* may be left as "INDEF". Otherwise setting it to the highest linear response level should yield better results. Obviously unrealistically low values (eg. negative) can be eliminated

by setting *datamin* to some low intensity threshold, though this is not necessary for good results. For an uncrowded field with no faint companion stars near stars of interest, one may confidently use the output of this Task as an accurate brightness catalogue without completing the next steps.

7. Build an accurate psf and magnitude set.

The procedures involving **psf** for crowded and uncrowded fields are different, but the execution of **psf** itself is the same. If running **psf** interactively, skip section A.

A) Preliminaries for the initial run of **psf**

pstselect *imname photflnm: pstname 500*

pstname is the output list of found psf candidate stars

500 is the maximum number of candidates one asks the Task to find

One is then prompted for *psfrad*, *fitrad*, *datamin* and *datamax*. The latter two should receive the same consideration as they did in **phot**; the former should be fine as they are. This Task searches the magnitude file produced by **phot** and outputs a file of stars meeting these criteria:

- no other stars should be within *fitrad* of a selected star
- any stars within 1.5 *psfrad* of a selected star should be fainter than it (neighbour stars)

The stars in this list may be identified in the image using **display**, **pdump**, and then **tvmark**. The command **pdump pstname XCENTER,YCENTER,MAG,ID yes > cooffnm** will produce the file *cooffnm* usable by **tvmark** to mark the stars. **display** is used to clear the old marks. Most of these stars should be removed from the file. No saturated stars should remain in the list, though a good selection close to saturation is desirable. A final set of 3-6 stars may be sufficient for a sparse field, 20-30

for a semi-crowded field, usually fewer than 60 for a significantly crowded field. The edited *pslname* file is an input for **psf**.

B) Running **psf** and **seepsf**

psf *imname photflnm pslname psfname nwpstnm grpflnm*

pslname is the input psf star list, it should be null (" " " ") if **psf** is run interactively

psfname is the output psf image

nwpstnm is the output list of psf stars

grpflnm is an output file for groups of stars (these are composed of psf stars and their neighbours)

The user will then be prompted for *function*, *varorder*, *psfrad*, *fitrad*, *datamin* and *datamax*. The *function* parameter specifies the underlying shape of the stellar profile (typically gaussian). The default values are fine for these parameters, except that *datamin* should be a large negative number (eg. -5000) so that **psf** can achieve a better fit. When **psf** is run noninteractively, the input stars are combined to make the psf without further work, so one may skip to the **seepsf** command.

- select the SAOimage window
- identify relatively isolated stars for the psf such that no other stars are within *fitrad* of a selected star, the selected stars are not saturated and any stars within 1.5 *psfrad* of a selected star are fainter than it (neighbour stars)
- a final set of 3-6 stars may be sufficient for a sparse field, 20-30 for a semi-crowded field, usually fewer than 60 for a significantly crowded field
- move to an appropriate star and press "a" to examine its suitability (if **psf** has an input psf star list, these will automatically be selected and one ignores selection using "a" until all initial stars are accepted or rejected according to the following steps)
- select the graphics window (tektronix/TeX) and position the cursor on the star
- press "c" to remove a gaussian fit and view the residuals

- when the residuals are dominated by sky fluctuations, press "o" again to add the star to the psf
- otherwise press "x" to reject the star
- select the SAOimage window and repeat for other stars
- when finished, select the SAOimage window and press "q"
- select the xterm window and press "w" to update the psf
- select the SAOimage window, press "q", select the xterm window, press "q" to exit

seepsf *psfname* *rpsfname*

rpsfname is the actual psf profile image

display *rpsfname* 1

seepsf and **display** are used to examine the quality of the psf after each run of **psf**. A good psf will look like a stellar image with no significant brightness patches outside the central core.

After running **psf**, it is a good idea to resort your stars to place the psf stars at the beginning of the file, followed by the remaining stars in order of increasing magnitude (ie. dimmest stars last). This facilitates editing stellar identifications later on. The sort may be accomplished as follows:

- type **psort** *daoffnm* MAG
- manually move psf stars up to the top of the list in *daoffnm*
- type **prenumber** *daoffnm*
- repeat the procedure used previously up to and including use of **psf**, making sure the psf stars selected are the same ones originally found.

C) Procedure for a crowded field

For a crowded field, **nstar** produces a magnitude file based on the psf image. The accuracy of the psf may then be checked using **substar**. Initially, **psf** should be run on the image, followed by **nstar**.

nstar *imname* *grpflnm* *psfname* *nstflnm* *nrjflnm*

nstflnm is the output file for accurate magnitudes
nrjflnm is the list of stars which **nstar** could not
fit properly

The user will then be asked whether or not to recenter the stars, refit the sky value and use group sky values. The responses should be "yes", "no" and "no". The user is also prompted for *psfrad*, *fitrad*, *maxgroup*, *datamax* and *datamin*, all of whose default values should be fine. Use **substar** on the original image to subtract the fitted stars.

substar *inname nstflnm excflnm psfname subname*

excflnm is the file containing the list of stars from
nstflnm to keep in the subtracted image; for the
initial run this should be null

subname is the output subtracted image

The user will then be prompted for *psfrad*, *datamin* and *datamax*, whose default values should be fine. The subtracted image should be examined for faint stars around the psf stars that were hidden from **daofind** by bright companions. Run **phot** interactively to select these new stars. Add the new photometry file *photflnm* to your catalog using **pconcat** and then renumber the stars with **prenumber**. Also, check through the stars in *nrjflnm* and remove any from the photometry file which might have been questionably identified or are not able to be handled by **nstar** (if they are too faint or close to the edge of the image or not found).

pconcat *infile outfile*

infile are files output by the same Task and are
separated only by commas

outfile is the resultant output file

pconcat requires the name of the Task which produced the input files. Type **eparam pconcat** to input the appropriate Task name (":q" exits the editing mode). Before **prenumber**, the input file must first be edited to remove header information

from the appended files (header info is preceded on each line by "#").

prenumber *infile*

infile is the input file

Rerun **substar** with *nwpstflnm* as *excflnm*. Run **psf** on this subtracted image to produce a better psf (use the same stars). Rerun **nstar** on the original image and check again with **substar**. Repeat the procedure (starting after the first run of **substar**) until the subtracted image is acceptable. Then run **allstar** as in section D to also get photometry on stars which aren't included in *grpflnm*.

D) Procedure for an uncrowded field

For an uncrowded field, one need only run **allstar** (which encompasses both the **nstar** and **substar** Tasks. If the subtracted image reveals hidden companions, then those are added to the coordinate and photometry files as in the crowded field procedure. Troublesome stars should also be deleted. Rerun **allstar** repeatedly, adding and deleting stars, until the subtracted image is satisfactory.

allstar *imname photflnm psfname allflnm arjflnm subname*

allflnm is the output file for magnitudes

arjflnm contains the list of stars not fit by **allstar**

The user will then be asked whether or not to recenter the stars, use group sky values and refit the group sky value. The responses should be "yes", "no" and "no". The user will also be prompted for *psfrad*, *ftrrad*, *maxgroup*, *datamin* and *datamax*, all of whose default values should be fine.

The **allstar** output file (*allflnm*) contains accurate magnitudes for all identified stars in the image. If there are stars in the image which are to remain, follow this procedure:

- type: **pdump** *allflnm* XCENTER,YCENTER,MAG,ID > *fcoo-
flnm*

- remove the stars you want to keep from *fcooffnm*
- use *fcooffnm* as *daoffnm* and run **phot** with *algorithm* set to “none” (you can do this either through **centerpars** or just answering the prompt when **phot** inquires as to its value)
- run **allstar** using the photometry file just created, answering “no” when the Task inquires about recentering the stars

APPENDIX C:

IRAF Irregular Aperture Photometry Procedures

(for an image with header file imname.imh)

This appendix contains detailed procedures for acquiring instrumental magnitudes for objects whose shapes are not roughly circular.

Initialisation:

- open a working window (`/usr/openwin/demo/xterm &` on **STELLAR**, `xgterm &` on **GALAXY**)
- open an "SAOimage" window (`/usr/local/bin/saoimage &` when on **STELLAR**, `saoimage &` on **GALAXY**)
- select the working window, "cd" to your IRAF directory (where your `login.cl` resides), and type "cl" to start IRAF from this window

1. Preprocess image (`noao` \rightarrow `imred` \rightarrow `ccdred`).

- see *IRAF Reduction Procedures* (Appendix A)

2. Display image (`images` \rightarrow `tv`).

display imname 1

imname is the image name

1 is the frame number (from 1-4)

3. Determine image parameters.

imstatistics imname[x1:x2,y1:y2]

- find a region free of stars, bounded by the coordinate set `x1`, `x2`, `y1`, `y2`
- record the sky brightness (mean) and fluctuations (standard deviation)

The values of sky brightness and deviations are determined as a default in the case of unusual apertures (shapes for objects).

4. Edit parameter files (**digiphot** → **apphot**).

datapars

- set *sigma* to background standard deviation
- set *threshold* to $5 \times \text{sigma}$
- set *ccdread* and *gain*, or *readnoise* and *epadu*
(*ccdread* and *gain* are header keywords, *readnoise* and *epadu* are numerical values in e^- 's and e^-/ADU)

polypars

- if the correct zero point to the magnitude scale for the appropriate filter is known, *zmag* should be set — otherwise the default value of 26.000 is fine

centerpars

- set *calgorithm* to “none”

fitscopypars

- set *salgorithm* to “mode” to measure the brightness of an object above the immediate surroundings, or to “constant” to measure the brightness with respect to *skyvalue*
- set *skyvalue* to sky brightness mean
- set *annulus* (inner radius of sky determination annulus) to just larger than the estimated maximum dimension of the irregular apertures to be used (not too large however, since the sky value becomes less meaningful farther away from the object in question)
- set *dannulus* (width of sky annulus; 10 is usually sufficient)

5. Catalogue aperture shapes, sizes and positions

polymark imname

At present, this Task is incapable of marking the polygonal apertures as they are constructed, so concentration and memory are important as one creates the list. Follow this procedure:

- select the SAOimage window and type "g"
- position the cursor at the first vertex of the polygon to be created and depress the space bar
- repeat for each vertex — **NB:** 1. the polygons are automatically closed (it is not necessary to come back to the first vertex, but remember the last side of the polygon will be a line from the last to first vertices); 2. **polyphot** integrates only the flux within the specified polygons
- type "q" to finish the polygon
- move the cursor to the point within the polygon which is to be used as the centre and depress the space bar
- if the polygon is generic enough to be used at other locations in the image, mark the other centres by moving the cursor and depressing the space bar, once per location
- to define other polygons, repeat this procedure
- to exit, type "q", select the IRAF working window, then type "q" again

Using the default values of the hidden parameters for **polymark**, the results will consist of two new files. *imname.coo.n* (where *n* is the version number of the file) contains the coordinates of the centre of each polygon followed by the centres of the alternate positions of that polygon (one per line) with a semicolon demarking a new polygon position set. If one has no polygons that are repeated in an image, this file may be ignored. File *imname.ver.n* contains a list of the polygons used. The coordinates of each vertex is a line in the file, and polygons are separated in the list by semicolons.

6. Determine instrumental magnitudes

Run **polyphot** noninteractively (eparam **polyphot**).

polyphot *imname* polygons=*imname.ver.n*

The default file read by **polyphot** is different than that written by **polymark** for the polygon list (an oversight by the programmers). This necessitates the setting of the *polygons* parameter

on the command line. The Task must be run twice if one wishes to measure brightness both with respect to the immediate surroundings and a constant level.

APPENDIX D:
IRAF Wide-Field Synthesis
(for images with header files imname.imh)

This appendix relates a detailed procedure for creating mosaics of many individual smaller images of the same size. NB: Large blocks of available memory are required.

Initialisation:

- open a working window (`/usr/openwin/demo/xterm &` on **STELLAR**, `xgterm &` on **GALAXY**)
- open an "SAOimage" window (`/usr/local/bin/saoimage &` when on **STELLAR**, `saoimage &` on **GALAXY**)
- select the working window, "cd" to your IRAF directory (where your `login.cl` resides), and type "cl" to start IRAF from this window

1. Perform reduction processing on the images

Component image frames relevant to the production of Wide-Field image should be processed as described in the Reduction Procedures outline (Appendix A). The names of the reduced frames should be placed in a file (one per line) called *flenm* such that they are in order from one corner of the Wide-Field to the opposite corner, successive images appearing along the rows or columns of the Wide-Field. (NB: The frames should only be trimmed to get rid of the overscan region. The images supplied to **irmosaic** MUST all be of the same dimensions.)

2. Edit the important parameter files (`noao` → `imred` → `irred`)

eparam irmosaic

- *trim_section* should be set to `[*,*]` to get the whole frame
- if there are gaps in the Wide-Field, specify the locations in *null_input* (eg. if images 3-5 and 10 are missing from the

sequence, enter 3-5,10 under *null_input*)

- *corner* is set to the corner of the Wide-Field matching the first frame in *flenm*
- *direction* is set to row or column (as per the order of the frames in *flenm*)
- *nxoverlap* and *nyoverlap* should be '0'
- *opixtype* should be equivalent to the input pixel type (generally real)

Component frames may be inverted horizontally, vertically or in both directions by replacing '*' by '-*' in *trim_section*. If there is a constant overlap (in pixels) and one is only going to use **irmosaic**, *nxoverlap* and *nyoverlap* may be set to the number of columns and rows that overlap in component frames. In this case, *subtract* should have the value 'yes'.

eparam irmatch2d

- *alignment* should be set to 'coords' for the initial run on a particular image, but may be 'file' for refinement runs
- *trimlimits* should be left blank unless subraster (component frame) trimming is desired (eg. for the removal of bad chip edges)
- *oval* should be set to a convenient level so that the features of the output image are clearly visible (a simple method is to type **imhistogram outfile** (*outfile* is the output image from **irmosaic**) and make *oval* a typical background value (on the low side of the peak) for the reference subraster)

The parameters *xref* and *yref* should be checked to see if the output image will be truncated. **irmosaic** picks a reference frame for its frame manipulations (by default, this is the middle frame in the list of frames; if the number of frames is even, then the reference is the leftmost of the middle two frames). By default, **irmatch2d** places the reference frame from the **irmosaic** output image in the same position (x and y coordinates) in the Wide-Field image. In some cases, especially those with very

large overlap, this positioning cuts off regions of the image. *xref* and *yref* give the shifts in pixels for the reference frame from its default position.

3. Construct the composite Wide-Field image

There are two possibilities; one's selection should depend upon the extent of overlap regions between individual component images. In the case of constant overlap (in pixels), one need only use *irmosaic* to complete the image. The only drawback is that it is not as easy to conveniently match intensities between component images. The second method is useful in that it works for variable overlaps. **NB:** Both options require the use of *irmosaic*. This Task only produces rectangular output images. If from the number of images you have you cannot form a simple rectangle, pad the input by repeating components in the sequence until a rectangle is possible.

A) Using *irmosaic* alone:

Set *nxoverlap* and *nyoverlap* to the size of the pixel shift in each direction (*eparam irmosaic*).

irmosaic @flenm outfile dbsfile numimx numimy

flenm is the file of component frame names

outfile is the output Wide-Field image

dbsfile is the output info database file

numimx is the number of components in a row

numimy is the number of components in a column

The output image background sky level will likely vary between component images. Run *imstatistics* on the component images. Pick a reference sky value and numerically add or subtract a constant from each of the other image sections in the mosaic using *imarith*.

B) For variable overlap regions:

irmosaic @*flenm outfile dbsfile numimx numimy*

To display an **irmosaic** output image, one generally needs a larger image buffer than one typically uses to display images. If one uses **SAOimage**, open a new display window (after exiting the previous **SAOimage** window) with the command **saoimage -gd xlenxylen**. This provides a window of 'xlen' by 'ylen' pixels so that one can see more than a 512x512 region at once without distortion by stretching the window. The size is limited by one's screen size. To allow a Wide-Field to be displayed completely, type 'set stdimage = imtpixsz' in the IRAF working window, where **pixsz** is the number of pixels on the longest axis of the Wide-Field images). This number of pixels should be the largest that one will use in one session of IRAF. CAUTION: if the value is too large, the time required to display images quickly becomes inconvenient. One may edit this line in one's **login.cl** file to preserve the change for the next use of IRAF.

display *outfile 1*

rimcursor > *posfile*

posfile is the output coordinate position file

When one occurs running **display**, check that the **images** and **AGES** are loaded in the **login.cl**. After entering the command (**rimcursor** is in the **Package lists** which are automatically loaded on entering IRAF), select the **SAOimage** package. One must then match stars in adjacent component images. Procedure: Select a star common to the first 2 component images. Move the cursor to that star in the first frame and hit the space bar. Wait a few seconds as **rimcursor** initiates a new write-to-file and then move the cursor to the same star in the second frame and hit the space bar. Matching 4 stars between adjacent frames should be sufficient. Proceed left to right in each row of frames and match each row of images to the one below, proceeding frame by frame along the row as you match the rows. Be careful to be consistent in the order of

recording of the pairs (ie. select a star in one frame, then go to the next frame, then select another star in the first frame, then in the second, etc.). Each time the view is changed using 'pan' (in SAOimage), the first space bar selection requires a few seconds for the initialisation of a write-to-file, subsequent space bar selections are essentially instantaneous. One exits this Task by hitting control-d.

itselect norm *posfile* none 0 1 1 1,2 *outpos*

outpos is the final output coordinate position file readable by **irmatch2d**

This Task was written by the author and is the subject of Appendix E. At present it can only be run on STELLAR, where one must load the **local** Package first to use it. The output produced by **rimcursor** contains extra information that the **itselect** Task will prune from the file. If there is a problem running **itselect**, check to see if the **nlocal** PACKAGE is loaded in the *login.cl*. Remember to set the *oval* parameter before running **irmatch2d**.

irmatch2d *outfile compimag dbsfile* (>> *temp.out*)

compimag is the Wide-Field composite image
temp.out is a file for the output messages from
irmatch2d

This command produces the Wide-Field composite image. It may be trimmed now to a smaller rectangular image if the usable area is small. If any problems occur, they will likely be due to a small consistency error in the coordinate file. The optional [>> *temp.out*] suffix to the **irmatch2d** command redirects processing messages to a file, appending new info to old.

If the Wide-Field image is not well matched in either intensity or coordinate shifts, corrections to the values used may be made by using the data in *temp.out*. These data are listed in the format:

InputFrameCoord UsedSection Δx Δy OutputCoord Δint

The x-shifts, y-shifts and intensity-shifts may be extracted to a

file with the command: **itselect** norm temp.out none 0 1 1 3,4,6
coords. The new data in *coords* may then be edited. The pa-
rameters *alignment* and *coords* should then be set to “file” and
coords respectively. The parameter *trimlimits* may also be al-
tered if one suspects that it is only the edges of the frames
which are causing problems ($[x1:x2,y1:y2]$ deletes columns $1 \rightarrow x1$,
 $(\max(x)-x2) \rightarrow \max(x)$ and rows $1 \rightarrow y1$, $(\max(y)-y2) \rightarrow \max(y)$).
Re-running **irmatch2d** produces a new image which may be
further corrected in the same manner.

APPENDIX E:

Itselect — A file manipulation Task

This appendix contains the source code (written in the IRAF programming language) and the IRAF-format “help page” for **itselect**. I developed this Task to manipulate and extract data from files in column or IRAF paragraph format. It was initially intended to handle specific IRAF data files through shortcuts to specific ends, though these features are as yet incomplete.

THE SOURCE CODE

```
# The itselect Task is written for the purpose of extracting information
# written in paragraph or table format from files written by IRAF Tasks
# (eg. phot). The information must be delimited by whitespace.

include <imhdr.h>
include <error.h>

define END "end"
define FIND "find"
define PHOT "phot"
define DAMP ".datatemp"
define SZ_SEL 4
define DECIMAL 10
define DEFAULT "default"
define MAX_RECS 10
define MAX_ITEMS 10
define OVERWRITE "overwrite"
define MAX_REC_PAR 20

procedure t_itselect()

pointer sp, input, inlist, line, item, n2list, endl, nendl,
        inpt2, im, numstr, recstr, rec[MAX_REC_PAR], it[MAX_ITEMS],
```

```

        outpt, file1, stflnm
char    broot[SZ_FNAME], select[SZ_SEL], datmag[SZ_LINE], suffix[SZ_LINE],
        datum[SZ_LINE]
int     jknnum, numrec, fd, nchar, i, j, outfd, nfiles,
        nimages, k, numitm, ip, items[MAX_ITEMS],
        recs[MAX_RECS], numrci, endlin, l
bool    append, overwrt

pointer imtopenp(), immap()
int     clpopni(), clgfil(), open(), clgeti(), ctowrd(), getline(),
        clplen(), imtgetim(), imtlen(), arrpti(), gctol()
bool    clgetb(), streq()

begin

call smark (sp)
call salloc (input, SZ_FNAME, TY_CHAR)
call salloc (line, SZ_LINE, TY_CHAR)
call salloc (item, SZ_LINE, TY_CHAR)
call salloc (inpt2, SZ_FNAME, TY_CHAR)
call salloc (numstr, SZ_LINE, TY_CHAR)
call salloc (recstr, SZ_LINE, TY_CHAR)
call salloc (outpt, SZ_LINE, TY_CHAR)
call salloc (endlin, SZ_LINE, TY_CHAR)
call salloc (nendlin, MAX_ITEMS, TY_LONG)
call salloc (file1, SZ_LINE, TY_CHAR)
call salloc (stflnm, SZ_LINE, TY_CHAR)
do k = 1, MAX_REC_PAR call salloc (rec[k], SZ_LINE, TY_CHAR)
do k = 1, MAX_ITEMS
call salloc (it[k], SZ_LINE, TY_CHAR)

# Get the Task parameters.
call clgstr ("select", select, SZ_SEL)
inlist = clpopni ("filenms")
nfiles = clplen (inlist)

```

```

if (streq (select, PHOT)) {
n2list = imtopenp ("imfiles")
nimages = imtlen (n2list)
if (nfiles != nimages) {
call printf ("WARNING: file and image list sizes do not match!!\n\n")
}
}

junknum = clgeti ("junknum")
if (streq (select, FIND)) {
numrec = 1
call clgstr ("itemnum", Memc[numstr], SZ_LINE)
numitm = arrpti (Memc[numstr], items, suffix, MAX_ITEMS)
do i = 1, numitm
recs[i] = 1
}

else {
numrec = clgeti ("numrecs")
if (numrec == 1) {
call clgstr ("itemnum", Memc[numstr], SZ_LINE)
numitm = arrpti (Memc[numstr], items, suffix, MAX_ITEMS)
do i = 1, numitm
recs[i] = 1
}
else {
call clgstr ("itemrec", Memc[recstr], SZ_LINE)
numrci = arrpti (Memc[recstr], recs, suffix, MAX_RECS)
if (numrci == 1) {
call clgstr ("itemnum", Memc[numstr], SZ_LINE)
numitm = arrpti (Memc[numstr], items, suffix, MAX_ITEMS)
do i = 2, numitm
recs[i] = recs[1]
}
else {

```

```

call clgstr ("itemnum", Memc[numstr], SZ_LINE)
numitm = arrpti (Memc[numstr], items, suffix, MAX_ITEMS)
}
}
;

call clgstr ("outflnm", Memc[outpt], SZ_LINE)
call clgstr ("procline", Memc[endl], SZ_LINE)
call clgstr ("outroot", oroot, SZ_FNAME)
append = clgetb ("append")
overwrt = clgetb ("overwrt")

# Print a message listing the number of files processed.
if (streq (select, PHOT)) {
call printf ("\n\nProcessing %d magnitude file(s) and %d image file(s)...\n\n")
call pargi (nfiles)
call pargi (nimages)
}
else {
call printf ("\n\nProcessing %d file(s)...\n\n")
call pargi (nfiles)
}

# Setting the end-of-processing point.
if (!streq (Memc[endl], END)) {
ip = 1
nchar = gctol (Memc[endl], ip, Meml[nendl], DECIMAL)
endlin = int(Meml[nendl]) + jknum
}
else
endlin = 999999999

# Opening files and processing selections.
call strcat (suffix, oroot, SZ_LINE)
if (append && streq (Memc[outpt], DEFAULT))

```

```

outfd = open (oroot, APPEND, TEXT_FILE)
else if (append)
outfd = open (Memc[outpt], APPEND, TEXT_FILE)
else if (streq (Memc[outpt], DEFAULT)) {
iferr (outfd = open (oroot, NEW_FILE, TEXT_FILE))
outfd = open (oroot, READ_WRITE, TEXT_FILE)
}

else {
iferr (outfd = open (Memc[outpt], NEW_FILE, TEXT_FILE))
iferr (outfd = open (Memc[outpt], READ_WRITE, TEXT_FILE)) {
call strcpy (DAMP, Memc[stflnm], SZ_LINE)
iferr (outfd = open (Memc[stflnm], READ_WRITE, TEXT_FILE))
outfd = open (Memc[stflnm], NEW_FILE, TEXT_FILE)
}
}

l=1
while (clgfil (inlist, Memc[input], SZ_FNAME) != EOF) {
fd = open (Memc[input], READ_ONLY, TEXT_FILE)
if (l == 1) {
call strcpy (Memc[input], Memc[file1], SZ_LINE)
if (streq (Memc[outpt], Memc[file1])) {
if (overwrt) {
call close (outfd)
call strcpy (DAMP, Memc[stflnm], SZ_LINE)
iferr (outfd = open (Memc[stflnm], READ_WRITE, TEXT_FILE))
outfd = open (Memc[stflnm], NEW_FILE, TEXT_FILE)
}
else if (append) {
call printf ("WARNING: Data is appended to first input file.\n")
call fprintf (outfd, "\n")
}
}
}

```



```

else {
call printf ("WARNING: The output file is the input file.\n")
call close (outfd)
call strcpy (DAMP, Memc[stfinm], SZ_LINE)
iferr (outfd = open (Memc[stfinm], READ_WRITE, TEXT_FILE))
outfd = open (Memc[stfinm], NEW_FILE, TEXT_FILE)
}
}
}

```

```

if (streq (select, PHOT)) {
if (numitm > 1) {
call close (fd)
call clpcls (inlist)
call sfree (sp)
call error (1,
"use ñormto access more than one item from phot files")
}
for (k=1; datmag[k] != EOS; k=k+1)
datmag[k] = NULL
if (imtgetim (n2list, Memc[inpt2], SZ_FNAME) != EOF) {
im = immap (Memc[inpt2], READ_ONLY, 0)
call imgstr (im, "DATETIME", datmag, SZ_LINE)
call imunmap (im)
}
j=0
while (getline (fd, Memc[line]) != EOF && j <= endlin) {
j=j+1
if (j-jnknum > (9*numrec)) {
call imtclose (n2list)
call close (fd)
call close (outfd)
call clpcls (inlist)
call sfree (sp)

```

```

call error (1, "too many comparison stars for this output")
}
if (j <= jnknum)
next
else if (mod (j-jnknum-recs[1],numrec) != 0)
next
ip = 1
for (i=1; i<=items[1]; i=i+1)
nchar = ctowrd (Memc[line], ip, Memc[item], SZ_LINE)
if (datmag[1] == NULL)
call strcat ("N/A", datmag, SZ_LINE)
call strcat (" ", datmag, SZ_LINE)
call strcat (Memc[item], datmag, SZ_LINE)
}
call fprintf (outfd, "%s\ n")
call pargstr (datmag)
}

```

```

else {
j=0
while (getline (fd, Memc[line]) != EOF && j <= endlin) {
j=j+1
if (j <= jnknum)
next
do k = 0, numrec-1 {
if (mod (j-jnknum,numrec) == k) {
if (k == 0)
call strcpy (Memc[line], Memc[rec[numrec]], SZ_LINE)
else
call strcpy (Memc[line], Memc[rec[k]],SZ_LINE)
}
}
if (mod (j-jnknum,numrec) == 0) {
for (k=1; datum[k] !=EOS; k=k+1)

```

```

datum[k] = NULL
do i = 1, numitm {
  ip = 1
  for (k=1; k<=items[i]; k=k+1) {
    nchar = ctowrd (Memc[rec[recs[i]]], ip,
    Memc[it[i]], SZ_LINE)
  }
  if (datum[1] != NULL)
    call strcat (" ", datum, SZ_LINE)
  call strcat (Memc[it[i]], datum, SZ_LINE)
}
call fprintf (outfd, "    ")
call pargstr (datum,
}
}
}
call close (fd)
l=l+1
}

call fprintf (outfd, "\n")
call close (outfd)
call clpcls (inlist)

if (overwrt && streq (Memc[outpt], Memc[file1])) {
  call delete (Memc[file1])
  call fcopy (Memc[stflnm], Memc[file1])
  call delete (Memc[stflnm])
}

if (streq (select, PHOT))
  call imtclose (n2list)
call sfree (sp)

```

```
call printf ("Processing complete. Output file is %s:\ n")
```

```
if (streq (Memc[outpt], DEFAULT)) {  
  call pargstr (oroot)  
} else if (streq (Memc[outpt], Memc[file1]) && !append && !overwrt) {  
  call pargstr (DAMP)  
} else {  
  call pargstr (Memc[outpt])  
}  
  
end
```

ARRPTI – Procedure to place integers from strings into an array.

```
int procedure arrpti (str, arr, ing, maxd)  
pointer tp, temp1, temp2  
char    str[ARB], ing[ARB]  
int     arr[maxd], maxd, i, ip, xp, arrsiz, nchar  
  
int     cctowd()  
long    gctol()  
  
begin  
  
  call smark (tp)  
  call salloc (temp1, SZ_LINE, TY_CHAR)  
  call salloc (temp2, maxd, TY_LONG)  
  
  ip = 1  
  for (i=1; i<=maxd && str[ip] != EOS; i=i+1) {  
    nchar = cctowd (str, ip, Memc[temp1], SZ_LINE)  
    if (i == 1)  
      call strcpy (Memc[temp1], ing, SZ_LINE)
```

```

else
call strcat (Memc[temp1], ing, SZ_LINE)
xp = 1
nchar = gctol (Memc[temp1], xp, Meml[temp2], DECIMAL)
arr1[i] = int(Meml[temp2]))
arrsiz = i
}

```

```

call sfree (tp)
return (arrsiz)

```

```

end

```

CCTOWD – Procedure to deconstruct a character string into tokens,
where tokens are delimited by whitespace OR commas.

```

include <ctype.h>
include <chars.h>

```

```

int procedure cctowd (str, ip, outstr, maxch)
char   str[ARB]           # input string
char   outstr[ARB]        # receives extracted token
int     ip                # pointer into input string
char    cch
int     maxch, ch, junk, op,
        ip_start, delim, i

```

```

int     cctoc()
define  qspat_ 91
define  wspat_ 92

```

```

begin

```

```

while (IS_WHITE(str[ip]) —— str[ip] == ',')

```

```

ip = ip + 1
ip_start = ip

delim = str[ip]
if (delim == DQUOTE ----- delim == SQUOTE) {
# Extract a quoted string.
op = 1
ip = ip + 1
do i = 1, ARB {
ch = str[ip]
if (ch == EOS) {
break
} else if (ch == ESCAPE) {
ch = str[ip+1]
if (ch == delim) {
ip = ip + 2
goto qsput_
} else {
junk = cctoc (str, ip, cch)
ch = cch
goto qsput_
}
} else if (ch == delim) {
ip = ip + 1
break
} else {
ip = ip + 1
qsput_      if (op <= maxch) {
outstr[op] = ch
op = op + 1
}
}
} else {
# Extract a whitespace or comma delimited string.

```

```

op = 1
do i = 1, ARB {
  ch = str[ip]
  if (IS_WHITE(ch) — ch == '\ 82 n' — ch == EOS — ch == ',') {
    break
  } else if (ch == ESCAPE) {
    junk = cctoc (str, ip, cch)
    ch = cch
    goto wspot_
  } else {
    ip = ip + 1
    wspot_      if (op <= maxch) {
    outstr[op] = ch
    op = op + 1
    }
  }
}

outstr[op] = EOS
return (ip - ip_start)

end

```

THE HELP FILE DESCRIPTION

NAME

itselect – manipulate IRAF and external data files

USAGE

itselect select flenms

PARAMETERS

select

The function to be completed. The selections are: “phot”, “find” and “norm”.

flenms

The data files to be processed. A file containing a file list or wildcards are allowed.

imfiles

The image files to be processed if “phot” is selected.

junknum

The number of lines skipped at the beginning of files. For phot files, the first 73 lines are commented out; for daofind files, the first 42 lines should be ignored in processing.

numrecs

The number of lines in a “paragraph” of data (eg. for one aperture, the phot Task produces 5 lines of data). A data file containing data in columns would have one line in a paragraph.

itemrec

The list of line numbers in each paragraph of data items that are to be extracted. They must be in the order of the desired output. If the selections are all from the same line, the line number must only appear once. Otherwise, for every item a line number must be given. They may be delimited by either spaces or commas.

itemnum

The list of item numbers to be selected from their respective lines. The list may be delimited by spaces or commas. For phot files, the magnitudes are in the 4th column of the last line of a paragraph.

outflnm = default

The output filename. The default filename is outroot followed by the item numbers of selections in the order that they appear in the output.

proclin = end

The number of lines to process after junknum lines have been skipped and the first line processed. This must be an integer multiple of numrecs, or "end" to proceed to the end of the file.

outroot = items

The rootname of the output file containing extracted data. The suffix attached to the rootname lists the item numbers from the original files in order that they are represented by columns in the new file (eg. if magnitudes are selected out of a daofind file, the output file will be "item3").

append = yes

Switch to append to an old output file or create a new file. The locations of new files just appended are identified by a blank line in the file.

overwrt = yes

Switch to overwrite the input file if flenms and outflnm are the same. If overwrt is "no", the data are moved to the file ".datatemp".

DESCRIPTION

The itselect Task is designed such that items may be selected from files containing extraneous information and put in columns in a new output file. This can aid in the processing of data by other programs and the ability to display the data with tools such as xvgr. Comment lines (headers) at the beginnings of files are not reproduced (using the junknum parameter). **WARNING:** Do not use this Task in a directory with a file

called “.datatemp”. This file may be deleted or overwritten. Data files with blank lines should be treated carefully. If there are blank lines used to delineate “paragraph”s, include them in the number of lines per paragraph. If the paragraph is one line, this is not necessary, but the blank lines will be reproduced in the output. Otherwise, blank lines should be removed or they will upset the Task’s line-counter.

Itselect identifies the locations of requested data items in the paragraph using the “coordinates” specified by itemrec and itemnum. These items are retrieved from the data files (files are processed in the order they would appear in a “dir — cat” command or the file containing their filenames) and printed in the output file in columns corresponding to the order in which they are listed in itemnum. This enables itselect to rearrange columns in a file, or to extract data from paragraphs in any requested order, without tedious and repetitive edit commands or the production of a new piece of code for each new file format.

The junknum and proclin features allow one to start from any point in the files to be processed and proceed to a specified line. Junknum should thus be the number of initial comment lines plus an integer multiple of the number of lines in a paragraph, for the Task to work properly. This allows the removal of sections of “unwanted” data from the entirety. Using the append switch is also helpful in this regard.

EXAMPLES

1. Extract star ID numbers and magnitudes from files produced by daofind.

```
lo> itselect find *.coo.*
Number of ignored lines at top of file (0:100): 42
Item number on selected line(s): 6 3
Output file name (default: outrootx1...xn): default

Processing 2 file(s)...
Processing complete. Output file is “items63”.
lo>
```

2. Do a “phot” procedure.

```

lo> itselect phot *.mag.*
List of associated images files: *.imh
WARNING: file and image list sizes do not match!!

Number of ignored lines at top of file (0:100): 73
Number of lines in a "paragraph" (1:20): 5
Line number of requested item(s): 5
Item number on selected line(s): 4
Output file name (default: outrootx1...xn): default

Processing 2 magnitude file(s) and 1 image file(s)...
Processing complete. Outout file is "items4".
lo>

```

3. Exchange two columns (1 and 5) in a file (test.dat) containing 5 data columns.

```

lo> itselect norm test.dat
Number of ignored lines at top of file (0:100): 0
Number of lines in a "paragraph" (1:20): 1
Item number on selected line(s): 5 2 3 4 1
Output file name (default: outrootx1...xn): default

Processing 1 file(s)...
Processing complete. Output file is "items52341".
lo>

```

BUGS At present the exposure date from images written by HPC-1 is not entirely transferred when this header parameter is read by IRAF. Thus, the exposure date is now limited to the day-of-the-week of the exposure. This should soon be rectified. Other functions should be available soon.

SEE ALSO

lists, lists.columns, proto.fields